

1 **Slow true polar wander around varying equatorial axes since 320 Ma**

2

3 **Bram Vaes^{1,2} and Douwe J.J. van Hinsbergen¹**

4 ¹Department of Earth Sciences, Utrecht University, Utrecht, The Netherlands

5 ²Department of Earth and Environmental Sciences, University of Milano-Bicocca, Milan, Italy

6

7 Corresponding author: Bram Vaes (bram.vaes@unimib.it)

8

9 **Key points:**

- 10 • New estimates of the magnitude and rate of true polar wander during the last 320 million years
- 11 • True polar wander mostly occurred about two nearly orthogonal equatorial axes
- 12 • No evidence for fast ($>1^\circ/\text{Ma}$) true polar wander rotations of >5 Ma since 320 Ma

13

14

15 **This paper is a non-peer reviewed manuscript submitted to EarthArXiv. The manuscript**

16 **has been submitted for peer review to *AGU Advances*.**

17 Abstract

18 True polar wander (TPW), the rotation of the solid Earth relative to the spin axis, is driven by changes
19 in the Earth's moment of inertia induced by mantle convection and may have influenced past climate
20 and life. Long-term TPW is typically inferred from large polar shifts in paleomagnetic apparent polar
21 wander paths or computed directly by rotating them in a mantle reference frame. However, most
22 apparent polar wander paths do not incorporate uncertainties in paleomagnetic data, which may bias
23 estimates of TPW. Here, we provide new quantitative estimates of TPW since 320 Ma by placing a
24 recent global apparent polar wander path corrected for age bias and with improved uncertainty
25 quantification in existing mantle reference frames. We find large amplitude ($>10^\circ$) but slow TPW
26 rotations that predominantly occurred about two equatorial axes that are approximately orthogonal.
27 During the Triassic and Jurassic, a $\sim 24^\circ$ TPW oscillation occurred about an axis at $\sim 15^\circ\text{W}$, close to the
28 present-day TPW axis at $\sim 10^\circ\text{E}$. In contrast, the TPW axis was located at $\sim 85^\circ\text{E}$ during a smaller
29 oscillation ($\sim 6\text{--}10^\circ$) over the past ~ 80 Ma, as well as between 260 and 320 Ma. We propose that these
30 varying TPW axes reflect changes in the distribution and flux of subduction in the Tethyan and Pacific
31 realms. We find no evidence for previously postulated fast ($>1^\circ/\text{Ma}$) TPW oscillations in the
32 Cretaceous and Jurassic. Finally, we propose that calibrating mantle convection models against
33 reconstructed TPW will improve our understanding of mantle dynamics and the drivers of TPW itself.

34

35 Plain Language Summary

36 True polar wander is the rotation of the Earth's crust and mantle relative to the spin axis. On geological
37 timescales, true polar wander is caused by movements of heavier or lighter material in the mantle,
38 such as sinking tectonic plates. To compensate for these movements, the Earth rebalances itself by a
39 rotation around an axis located on the equator. These rotations change the position of all continents
40 simultaneously, influencing their latitude and potentially climate and life. Additionally, the location of
41 the axis and the speed of true polar wander can provide important insights on the structure and
42 movement of material in the Earth's mantle. In this study, we calculated the magnitude, speed, and
43 axis of true polar wander for the last 320 million years. Our results suggest that while the rotations
44 were large ($>10^\circ$), they were relatively slow. True polar wander mainly occurred around two different
45 equatorial axes: one close to the present-day axis and the other about 90° away. The changing axis
46 may be caused by changes in the location and amount of sinking tectonic plates over time. Lastly, we
47 propose that models of mantle convection could help us better understand the drivers of true polar
48 wander.

49 **1 Introduction**

50 Determining the rate of convection of the Earth's mantle is key in deciphering the drivers of plate
51 tectonics and volcanism but is notoriously difficult to quantify from kinematic observations alone.
52 True polar wander (TPW) provides an avenue to kinematically constrain mantle convective processes.
53 TPW is the rotation of the Earth's mantle and crust (i.e., the solid Earth) relative to the spin axis, such
54 that the axis of maximum nonhydrostatic moment of inertia remains closely aligned with the spin axis.
55 On geological timescales, TPW is driven by the redistribution of density anomalies within the Earth's
56 mantle (Goldreich & Toomre, 1969; Evans, 2003), which include sinking subducted slabs or rising
57 mantle plumes (Steinberger and Torsvik, 2010). TPW rotations occur, by definition, about an axis
58 located in the equatorial plane, bringing excess masses towards the equator and mass deficits towards
59 the geographic poles (Gold, 1955; Evans, 2003). The magnitude and rate of TPW are primarily
60 controlled by the spatial distribution and magnitude of mass heterogeneities and by the viscosity of
61 the mantle (e.g., Spada et al., 1992; Tsai & Stevenson, 2007; Rose & Buffett, 2017). Quantitative
62 estimates of TPW therefore provide kinematic constraints on the structure, rheology, and dynamics
63 of the Earth's mantle. The primary tool to quantify TPW is paleomagnetism (e.g., Besse et al., 2021).
64 However, estimates of TPW obtained through paleomagnetism vary significantly, and the magnitude
65 and rate at which TPW occurred in the geological past are uncertain.

66 Long-term (≥ 5 Ma) TPW is often quantified using apparent polar wander paths, which track
67 the motion of the time-averaged paleomagnetic pole, assumed to coincide with the Earth's spin axis,
68 relative to a tectonic plate (e.g., Besse and Courtillot, 2002; Torsvik et al., 2008). Phanerozoic TPW
69 rotations have been determined by identifying common rotations of major continents observed from
70 paleomagnetic data (e.g., Jurdy & Van der Voo, 1974; Steinberger & Torsvik 2008; Torsvik et al., 2012,
71 2014). This approach has yielded relatively slow ($< 1^\circ/\text{Ma}$) TPW rates, but large in amplitude (up to
72 $> 20^\circ$ in the Paleozoic and Mesozoic; Torsvik et al., 2014). On the other hand, rapid shifts in the position
73 of the paleomagnetic pole have also been interpreted as evidence for fast TPW ($> 1^\circ/\text{Ma}$). Proposed
74 episodes of fast TPW include a short-lived episode at ~ 84 Ma (Gordon, 1983; Sager & Koppers, 2000;
75 Mitchell et al., 2021), a $\sim 30\text{-}40^\circ$ polar shift during the Late Jurassic referred to as the 'Jurassic monster
76 polar shift' (e.g., Kent & Irving, 2010; Kent et al., 2015; Muttoni & Kent, 2019), a $\sim 50^\circ$ polar shift in the
77 Ordovician-Silurian (Jing et al., 2022) as well as a $\sim 90^\circ$ degrees oscillation in the Ediacaran (e.g.,
78 Mitchell et al., 2011; Robert et al., 2017). The occurrence of such fast and large amplitude TPW events
79 not only has large implications for the structure and dynamics of the Earth's interior but may also
80 have had profound consequences for e.g., the biosphere, sea level, climate and the geodynamo (e.g.,
81 Evans, 2003; Raub et al., 2007; Biggin et al., 2012; Muttoni et al., 2013; Jing et al., 2022; Domeier et al.,
82 2023; Wang & Mitchell, 2023). However, the existence of these fast TPW episodes requires high-
83 resolution paleomagnetic data with small age uncertainties and therefore remains controversial:
84 several recent studies have questioned whether these polar shifts truly represent rapid TPW or rather

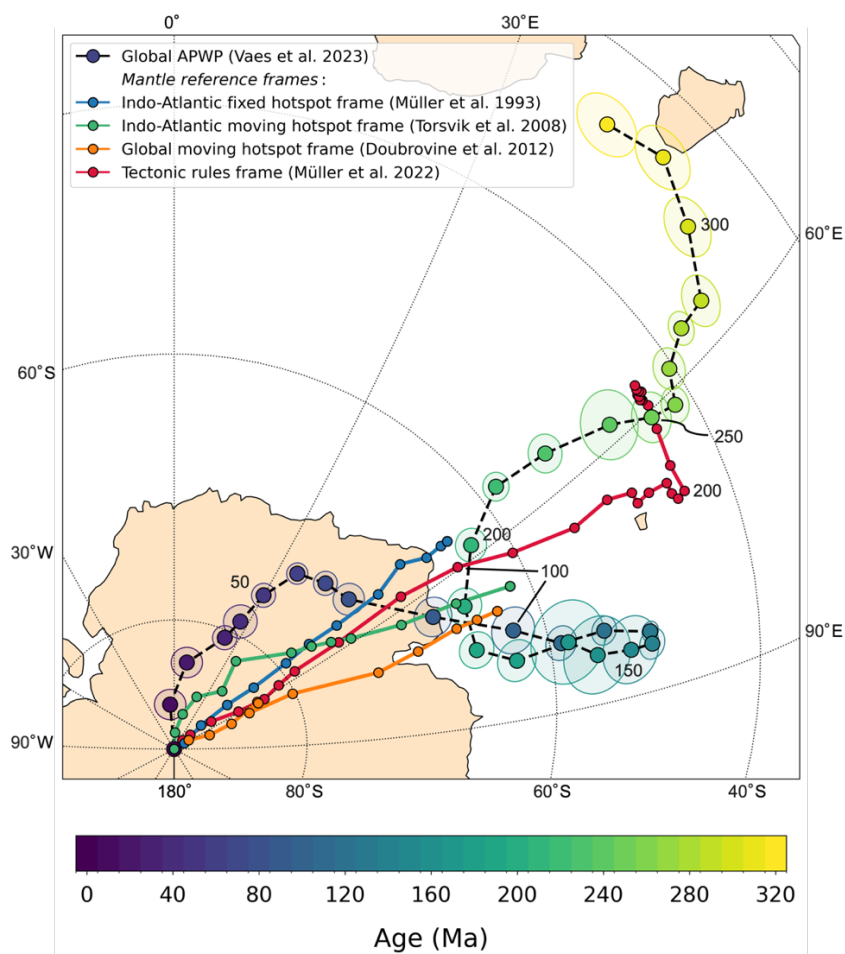
85 represent paleomagnetic artifacts, noise, or non-dipole behavior of the Earth's magnetic field (e.g.,
86 Kulakov et al., 2021; Cottrell et al., 2023; Domeier et al., 2023).

87 The most direct way to quantify the rate and magnitude of TPW is through the comparison of
88 paleomagnetic reference frames derived from an APWP and mantle reference frames that estimate
89 plate tectonic motions relative to the ambient mantle, such as a hotspot reference frame (e.g.,
90 Livermore et al., 1984; Andrews, 1985; Besse & Courtillot 2002; Doubrovine et al., 2012). Placing an
91 APWP in a mantle reference frame enables the construction of a TPW path that provides a direct
92 estimate of the motion between the spin axis and 'mean' solid Earth. However, the record of well-
93 defined hotspot tracks so far limited the reliable application of this approach to computing TPW back
94 to the Early Cretaceous (~120 Ma; Torsvik et al., 2008; Doubrovine et al., 2012). Studies using the
95 most recent hotspot reference frames obtained TPW paths that show slow ($<1.0^\circ/\text{Ma}$) but significant
96 (up to $10\text{-}20^\circ$ in magnitude) TPW back to Mesozoic times (e.g., Besse & Courtillot, 2002; Doubrovine
97 et al., 2012).

98 A clear limitation of most published estimates of TPW is that they were obtained using
99 conventional, pole-based apparent polar wander paths, in which spatial and temporal uncertainties
100 in the underlying data were not incorporated (e.g., Besse & Courtillot, 2002; Torsvik et al., 2012). The
101 recent global APWP of Vaes et al. (2023) is the first in which these sources of uncertainty were
102 propagated. One of the key steps forward of that global APWP is that estimates of APW rates may now
103 be corrected for temporal bias, by computing the 'effective' age of the reference pole positions of the
104 APWP from the age distribution of the paleomagnetic data used as input for those poles. Vaes et al.
105 (2023) showed that observed peaks in APW rate that have previously been interpreted as phases of
106 relatively rapid TPW, such a spike between 110 and 100 Ma (Steinberger & Torsvik, 2008; Torsvik et
107 al., 2012; Doubrovine et al., 2012), disappeared after correcting for the 'effective' age difference
108 between successive reference poles of the APWP.

109 Here, we derive new quantitative estimates of the magnitude, direction, and rate of TPW since
110 320 Ma by comparing the recent global APWP of Vaes et al. (2023) with previously published mantle
111 reference frames. We first compute TPW paths that track the motion of the time-averaged
112 paleomagnetic pole relative to the deep mantle for the last 120 Ma using mantle frames based on
113 hotspots with different underlying assumptions (Müller et al., 1993; Torsvik et al., 2008; Doubrovine
114 et al., 2012). Next, we compute TPW back to 320 Ma using a recent mantle reference frame of Müller
115 et al. (2022) that is based on a set of tectonic 'rules' and was computed for the last 1 Ga. We test
116 previous observations that show that TPW was limited since the mid-Cretaceous and analyze whether
117 the axis of TPW has remained approximately stable, as previously proposed, or whether TPW
118 rotations occurred around changing equatorial axes since 320 Ma. Next, we re-assess whether fast
119 polar shifts that were previously interpreted as phases of TPW may truly represent rapid TPW or
120 rather may have resulted from noise induced by age uncertainty or the use of paleopole averages in
121 determining polar wander. Finally, we discuss the implications of our results for analyzing mantle
122 dynamics and the role of deep-mantle structure in determining the axis of TPW.

123



124

125 **Fig. 1.** Comparison between the global APWP for the last 320 Ma of Vaes et al. (2023) and the four
 126 mantle reference frames used in this study to derive TPW. The global APWP is plotted in South African
 127 coordinates, thus showing the position of the Earth's spin axis relative to a fixed South Africa. The pole
 128 positions were computed at 10 Ma steps using a 20 Ma sliding window (Fig. S1, Table S2). Reference
 129 poles and 95% confidence regions are colored by their age. The four polar wander paths constructed
 130 using the mantle reference frames indicate the motion the 'mean' mantle relative to a fixed (South)
 131 African plate (Table S3). In the absence of TPW, this would correspond to the motion of the spin axis
 132 relative to the Africa plate. Note that these paths based on the mantle reference frames only go back
 133 to 120 Ma, except for the tectonic rules frame of Müller et al. (2022), which is plotted here back to 320
 134 Ma.

135

136 2 Methods

137 We construct true polar wander paths (TPWPs) using four different mantle reference frames (Fig. 1,
 138 Table S1): the Indo-Atlantic fixed hotspot reference frame of Müller et al. (1993), the Indo-Atlantic
 139 moving hotspot reference frame of Torsvik et al. (2008), the global moving hotspot reference frame
 140 of Doubrovine et al. (2012), and the recently published mantle reference frame of Müller et al. (2022)

141 that was constructed using an optimization approach based on a set of ‘tectonic rules’ (Tetley et al.,
142 2019). We computed each TPWP as an apparent polar wander path in a coordinate frame in which the
143 mantle is kept fixed, following the approach of many previous workers (e.g., Livermore et al., 1984;
144 Andrews, 1985; Besse & Courtillot, 2002; Doubrovine et al., 2012). To this end, we placed the recent
145 global APWP of Vaes et al. (2023) in each of the mantle reference frames. We computed the TPWPs
146 using a time step of 10 Ma, which is the temporal resolution at which both paleomagnetic and mantle
147 reference frames are typically computed, as well as estimates of TPW that are derived from those (e.g.,
148 Steinberger & Torsvik, 2008; Torsvik et al., 2014). To account for the uneven age distribution of the
149 paleomagnetic input data, Vaes et al. (2023) computed the ‘effective’ age of the reference poles and
150 showed that this age is often significantly different from the center age of the 20 Ma time window used
151 to compute each reference pole. To construct a global APWP at exact 10 Ma time steps, we re-
152 computed the global APWP here using same paleomagnetic database, global plate circuit and iterative
153 approach used by Vaes et al. (2023). As an additional step, we interpolated between the reference
154 poles generated for each iteration to obtain a cloud of simulated reference poles with the same age
155 (e.g., 10, 20, 30 Ma; Fig. S1). We emphasize that in this approach, both the spatial and temporal
156 uncertainties in the underlying paleomagnetic data are propagated into the confidence regions of the
157 global APWP. We quantify the 95% confidence regions of this interpolated APWP by the P_{95} cone of
158 confidence, which includes 95% of the simulated reference poles computed for each time step,
159 following the approach developed by Vaes et al. (2022, 2023) (Fig. S1). Finally, to compute the TPWPs,
160 we placed the interpolated global APWP in each mantle reference frame by rotating it using the Euler
161 rotation poles (defined at 10 Ma steps) that describe the motion of the South African plate relative to
162 the mantle. The resulting polar wander path then describes the motion of the time-averaged
163 paleomagnetic pole relative to the ambient mantle, in the same way as a conventional APWP describes
164 the motion of the pole relative to a fixed tectonic plate.

165 It is important to note that in our computation of the TPWP, the uncertainties associated with
166 the mantle reference frames are not (yet) incorporated. The uncertainties of the rotation poles for
167 Africa relative to the mantle were not quantified for the fixed hotspot reference frame of Müller et al.
168 (1993) and the tectonic rules frame of Müller et al. (2022). 95% confidence regions for the two moving
169 hotspot reference frames were provided by Doubrovine et al. (2012) and Torsvik et al. (2008). In
170 addition, we note that the plate circuit and time scale used to determine the mantle reference frames
171 differs between all four models and is also different from the updated plate circuit as well as the time
172 scale (of Gradstein et al., 2020) used for the construction of the global APWP of Vaes et al. (2023).
173 Because the four reference frames are based on different input datasets, underlying assumptions, and
174 methodologies, they each provide a different perspective on the motion of South Africa relative to the
175 deep mantle.

176 The three hotspot-based mantle frames used here are assumed to determine the ‘absolute’
177 motion of tectonic plates relative to the deep mantle using hotspot tracks: linear chains of intraplate
178 volcanoes that show a clear progression of eruption ages (e.g., Wilson, 1963; Morgan, 1971; 1981).

179 The geometry and age progression of these hotspot tracks have been widely used to reconstruct
180 lithospheric motions relative to mantle upwellings (or ‘plumes’, Morgan, 1971), which are either
181 assumed to be stationary in a ‘mean mantle’ frame (i.e., a fixed hotspot reference frame, e.g., Morgan,
182 1981; Müller et al., 1993) or corrected for slow relative motions using a numerical model of mantle
183 convection (i.e., a moving hotspot reference frame; O’Neill et al., 2005; Torsvik et al., 2008; Doubrovine
184 et al., 2012). Moving hotspot reference frames, however, do not provide independent kinematic
185 constraints on mantle dynamics because a mantle convection model, constrained by a global model of
186 plate tectonic motions and mantle density heterogeneities, is used as input, after which the reference
187 frame is iteratively constructed to fit hotspot tracks (e.g., Torsvik et al., 2008; Doubrovine et al., 2012).
188 In addition, the disadvantage of hotspot reference frames is that the availability of linear hotspot
189 tracks only allows the determination of plate motions relative to hotspots back to the Early Cretaceous
190 (~120 Ma).

191 The recent mantle reference frame of Müller et al. (2022) was constructed in an entirely
192 different way. Building on the work of Tetley et al. (2019), they used an iterative approach in which
193 the absolute plate motion of the reference plate Africa is obtained by optimizing a global plate model
194 using four different criteria. These criteria include the restriction of the net lithospheric rotation rate
195 to values deemed reasonable from numerical experiments, the minimization of global trench
196 migration velocities, a global continental median plate velocity below 6.0 cm/a, and the minimization
197 of the spatio-temporal misfit between observed and model-predicted hotspot tracks (only used for
198 the last 80 Ma). We note that this type of mantle frame may be biased by subjective choices related to
199 the relative weighting of the different rules and the imposed limits. On the other hand, the joint
200 incorporation of multiple kinematic constraints enables the construction of a mantle frame that is less
201 likely to suffer from errors in or the overfitting of a single kinematic observation such as a hotspot
202 track (Tetley et al., 2019). Using the global plate model for the last billion years of Meredith et al. (2021)
203 as input for their model, Müller et al. (2022) constructed a tectonic rules-based mantle reference
204 frame since 1000 Ma, using 5 Ma time steps. No attempts were made to quantify the uncertainties for
205 this frame, however. Nonetheless, taking this frame at face value enables the computation of a TPW
206 path from 320 Ma to present, using the global APWP for the last 320 Ma of Vaes et al. (2023). Finally,
207 to assess whether fast TPW phases may have occurred during the last 320 Ma, we also computed a
208 TPWP at a 5 Ma resolution, following the same procedure as described above, but using the 5-Ma-
209 resolution-APWP of Vaes et al. (2023) instead.

210

211 **3 Results**

212 **3.1 True polar wander paths for the last 120 Ma**

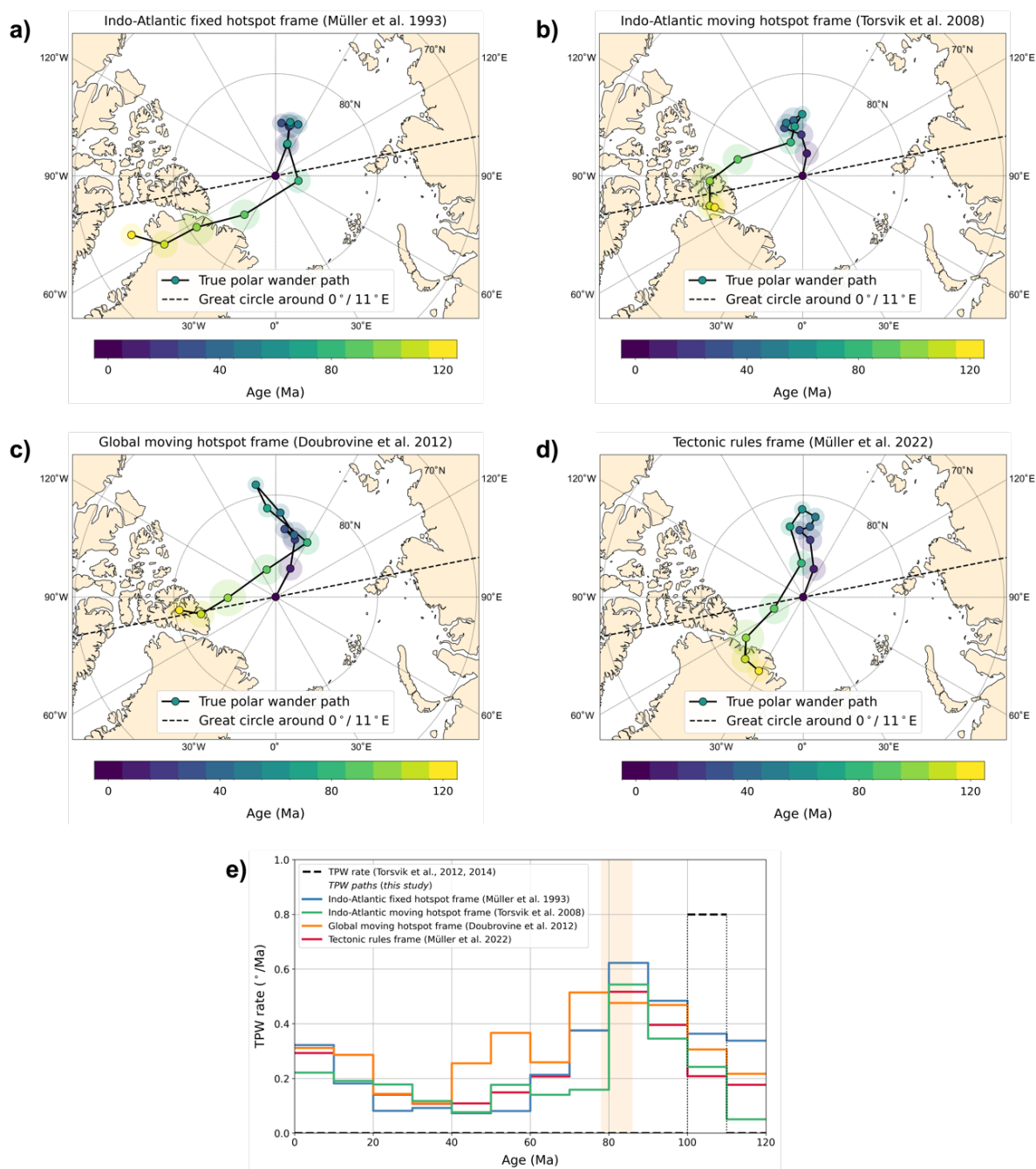
213 We first computed four true polar wander paths for the last 120 Ma using the four different mantle
214 reference frames (Fig. 2, Table S3). The paths show the motion of the time-averaged paleomagnetic
215 pole position, which is assumed to coincide with the spin axis, relative to the ‘mean’ mantle. The

216 TPWPs thus visualize the motion of the spin axis in a fixed mantle frame, providing direct estimates
 217 of the magnitude, rate, and direction of TPW. The four TPWPs show a similar first-order geometry for
 218 the last 120 Ma (Fig. 2a-d). All four paths show a back-and-forth motion of the spin axis during the last
 219 80 Ma, roughly along the 180° meridian. From 80 to 60 Ma, all paths show a shift in the pole position
 220 away from the geographic pole (in a fixed mantle frame), with the net TPW angle peaking at 60 Ma in
 221 all four TPWPs. Except for the path based on the global moving hotspot reference frame of Doubrovine
 222 et al. (2012), a near stillstand of the pole position is observed between 60 and 30 Ma, as indicated by
 223 the TPW rate of $\sim 0.1^\circ/\text{Ma}$ (Fig. 2e). The net angle of TPW of $>10^\circ$ at 60 Ma is notably larger for the
 224 Doubrovine et al. (2012) model than the $\sim 6^\circ$ for Müller et al. (1993) and Torsvik et al. (2008) models.
 225 The three TPW paths based on a hotspot reference frame show a sharp cusp at 80 Ma. Prior to 80 Ma,
 226 the trajectory of the TPWPs based on the Müller et al. (1993) and Doubrovine et al. (2012) frames is
 227 sub-parallel to the great circle around an equatorial TPW axis at 11°E, which is the proposed long-
 228 term TPW axis of Torsvik et al. (2014) that closely corresponds to the present-day axis of TPW
 229 (Pavoni, 2008). The TPWP computed using the Torsvik et al. (2008) frame shows a similar direction
 230 between 80 and 100 Ma but is perpendicular to this direction between 100 and 120 Ma. We observe
 231 very similar TPW rates for all four paths (Fig. 2e). For most of the last 120 Ma, including the entire
 232 Cenozoic, the TPW rate is between $\sim 0.1^\circ/\text{Ma}$ and $0.4^\circ/\text{Ma}$. The highest TPW rates are obtained for the
 233 Late Cretaceous, peaking at a rate of $0.5\text{-}0.6^\circ/\text{Ma}$. Notable, we find that the TPW rate since 120 Ma –
 234 on a timescale of 10 Ma - stays well below $1.0^\circ/\text{Ma}$, which we defined as the threshold for ‘fast’ TPW,
 235 following Cottrell et al. (2023).

236

237 **3.2 A true polar wander path back to 320 Ma**

238 We computed a TPWP back to 320 Ma by placing the interpolated global APWP of Vaes et al. (2023)
 239 in the tectonic rules frame of Müller et al. (2022) (Fig. 3, Table S4). The resulting TPWP can be roughly
 240 divided into five segments (Fig. 4a). For the last 130 Ma, the TPW path shows an oscillatory motion
 241 with a cusp at 60 Ma. During this time interval, the path runs approximately parallel to the 5°W
 242 meridian, depicted in Fig. 4a by the red line. The Jurassic-Triassic portion of the TPWP shows two
 243 smooth segments, from 130 to 200 Ma and from 200 to 260 Ma, that are nearly parallel. The trajectory
 244 corresponds to successive large TPW rotations around an equatorial axis located at $\sim 15^\circ\text{W}$ (blue line
 245 in Fig. 4a). During both these time spans, the spin axis is estimated to move $\sim 24^\circ$ relative to the stable
 246 mantle. Note that the position of the spin axis relative to a fixed mantle is close to the present-day
 247 position at 260-250 Ma, just before the large back-and-forth TPW rotations. The oldest part of the
 248 TPWP, from 260 to 320 Ma, runs roughly parallel to the 5°W/175°E meridian, similar to the 0-130
 249 Ma segments. The largest net TPW angle of approximately 21° is computed at 200 Ma and 320 Ma. The
 250 TPW rates computed for the last 320 Ma stay below $0.7^\circ/\text{Ma}$ for this entire time span, with an average
 251 of $0.34^\circ \pm 0.14^\circ/\text{Ma}$ (1σ).

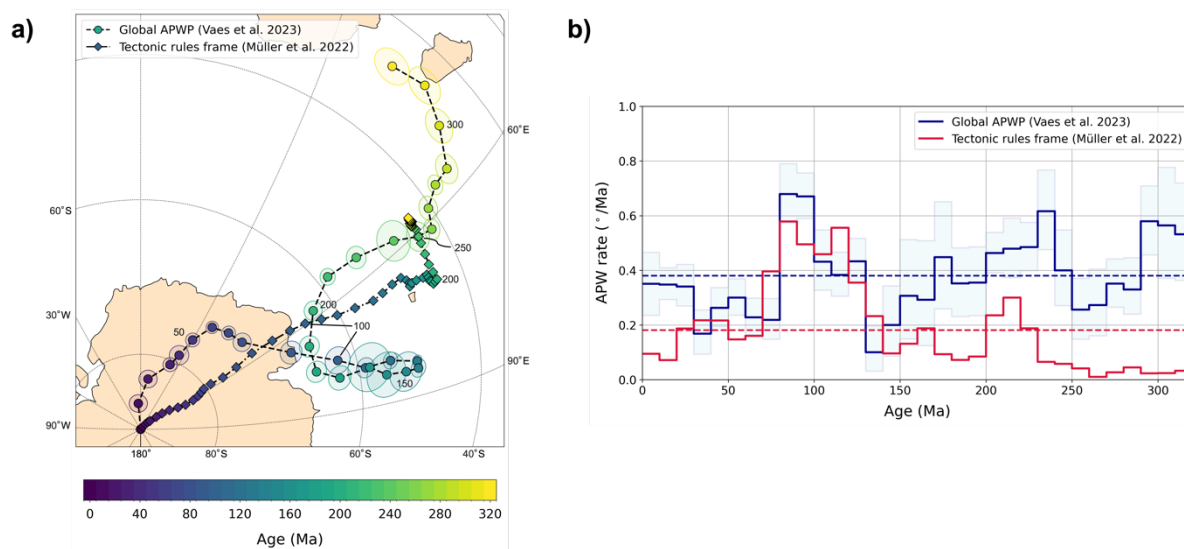


252

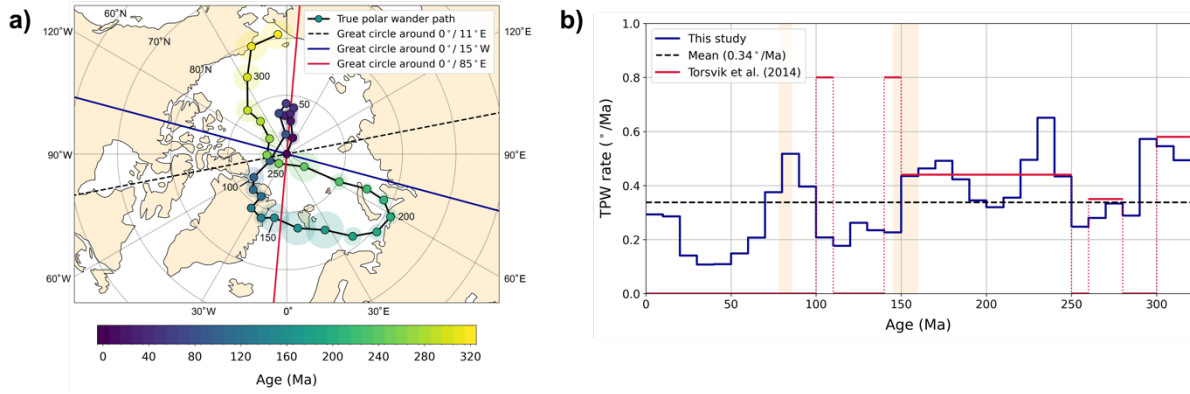
253 **Fig. 2.** True polar wander paths for the last 120 Ma, computed using four different mantle reference
 254 frames (a-d). The poles represent the location of the Earth’s spin axis relative to a fixed ‘mean’ mantle
 255 frames (a-d). The poles represent the location of the Earth’s spin axis relative to a fixed ‘mean’ mantle
 256 uncertainty only (that is, the P₉₅ of the reference frame (Müller et al. 1993) poles of the global APWP, see Vaes et al., 2023). The
 257 dashed black line shows the great circle around an equatorial rotation axis at 11°E, corresponding to
 258 the preferred TPW axis of Torsvik et al. (2012, 2014). The TPWPs are listed in Table S4. e) TPW rate
 259 for the last 120 Ma, estimated from each of the four TPW paths. The proposed phases of rapid TPW
 260 between 86 and 78 Ma by Mitchell et al. (2021) and between 110 and 100 Ma by Torsvik et al. (2012,
 261 2014) are indicated by the colored band and dashed black line, respectively.

262

263 The TPWP computed at a 5 Ma resolution shows a similar overall trend but is more irregular
 264 and has much larger confidence regions (Fig. 5, Table S5). Again, we emphasize that these confidence
 265 regions are solely defined by the uncertainty in the global APWP and do not incorporate those of the
 266 mantle reference frame – the true uncertainty must thus be larger. This is a direct consequence of the
 267 lower amount of paleomagnetic data that underlies each pole position, given that a smaller time
 268 window of 10 Ma is used instead of 20 Ma. The main difference with the 10 Ma-resolution TPWP is
 269 that there are segments of the path showing a zig-zag pattern, for instance between 10 and 60 Ma (Fig.
 270 5a). However, whether these motions are truly representative of TPW is questionable considering the
 271 relatively large and often overlapping (minimum) confidence regions. The larger uncertainty is also
 272 clearly reflected in the confidence regions of the APW rate of the 5-Ma-resolution-APWP (Fig. 5b). The
 273 TPW rates obtained from this higher resolution TPWP are $\sim 50\%$ higher than for the 10-Ma-resolution
 274 path, with a mean rate of $0.50^\circ \pm 0.27^\circ/\text{Ma}$ (Fig. 5c). In addition, five peaks are observed with a TPW
 275 rate of $>0.8^\circ/\text{Ma}$, with three peaks above $>1.0^\circ/\text{Ma}$. It should be noted, however, that the latter peaks
 276 are observed for the pre-260 Ma portion of the TPWPs, where the 5 Ma-resolution-APWP is the least
 277 robust and where the tectonic rules mantle frame likely has higher uncertainty than for younger times.
 278
 279

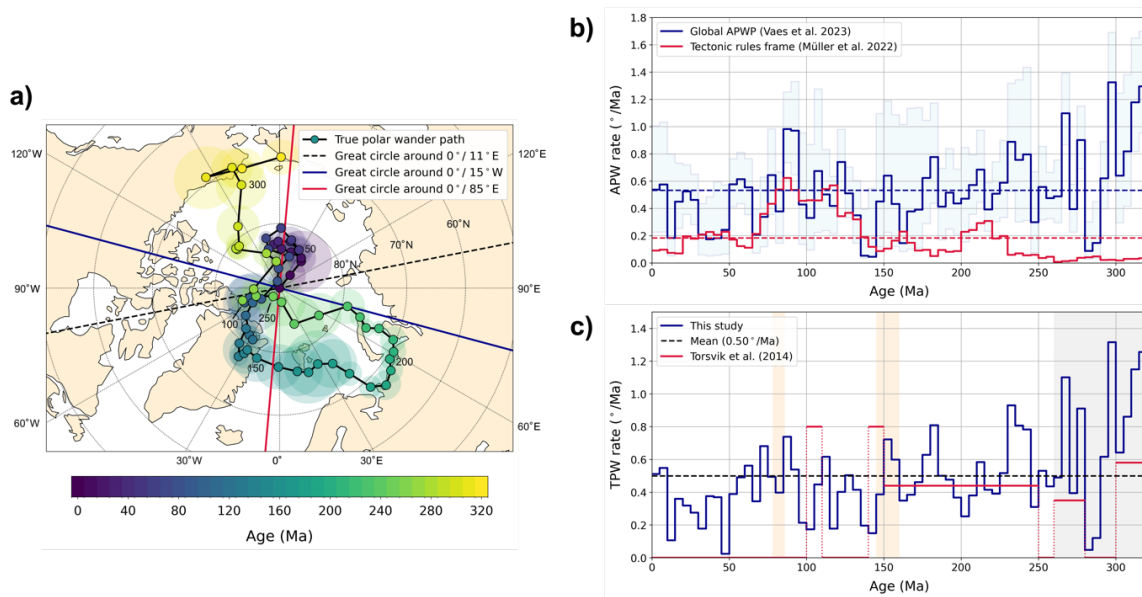


280
 281 **Fig. 3. a)** Orthographic plot of the global APWP of Vaes et al. (2023) and the tectonic rules mantle
 282 reference frame of Müller et al. (2022). The poles indicate the position of the Earth's spin axis and
 283 'mean' mantle relative to a fixed African plate, respectively. **b)** Comparison of the apparent polar
 284 wander rate derived from the pole paths shown in a). The horizontal dashed lines show the mean rate
 285 for the last 320 Ma. The light blue band indicates the 95% confidence regions on the rate that is
 286 computed from the uncertainty of the global APWP.



287

288 **Fig. 4. a)** True polar wander path for the last 320 million years, computed using the tectonic rules
 289 reference frame of Müller et al. (2022). Colors and confidence regions are the same as in Fig. 2. Great
 290 circles around three different TPW axes are shown in blue, red and black (dashed) lines, respectively.
 291 **b)** The estimated rate of TPW since 320 Ma, computed from the TPW path shown in a). The mean TPW
 292 rate ($0.34^\circ/\text{Ma}$) is indicated by the black dashed line. Previously inferred TPW rates by Torsvik et al.
 293 (2024) are shown in red. Note that this study identified multiple ‘phases’ of TPW, interspersed by time
 294 intervals without significant TPW. Time intervals for which rapid TPW ($>1^\circ/\text{Ma}$) has been proposed
 295 are highlighted by the colored bands.



296

297 **Fig. 5. a)** TPW path computed at a 5 Ma resolution using the global APWP from Vaes et al. (2023)
 298 calculated at a 5 Ma time step using a 10 Ma time window (Table S5). **b)** Comparison of the polar
 299 wander rates derived from the 5-Ma resolution global APWP and tectonic rules mantle frame of Müller
 300 et al. (2022). The horizontal dashed lines show the mean rates. The light blue band indicates the 95%
 301 confidence regions on the rate that is computed from the uncertainty in the 5 Ma-resolution global
 302 APWP. **c)** Same as Fig. 4c, but now showing the TPW rate derived from the 5-Ma-resolution TPW path
 303 shown in a). The grey area highlights the time interval for which the TPW path is less robust, leading
 304 to large variations in TPW rate that are likely the result of noise.

305 **4. Discussion**

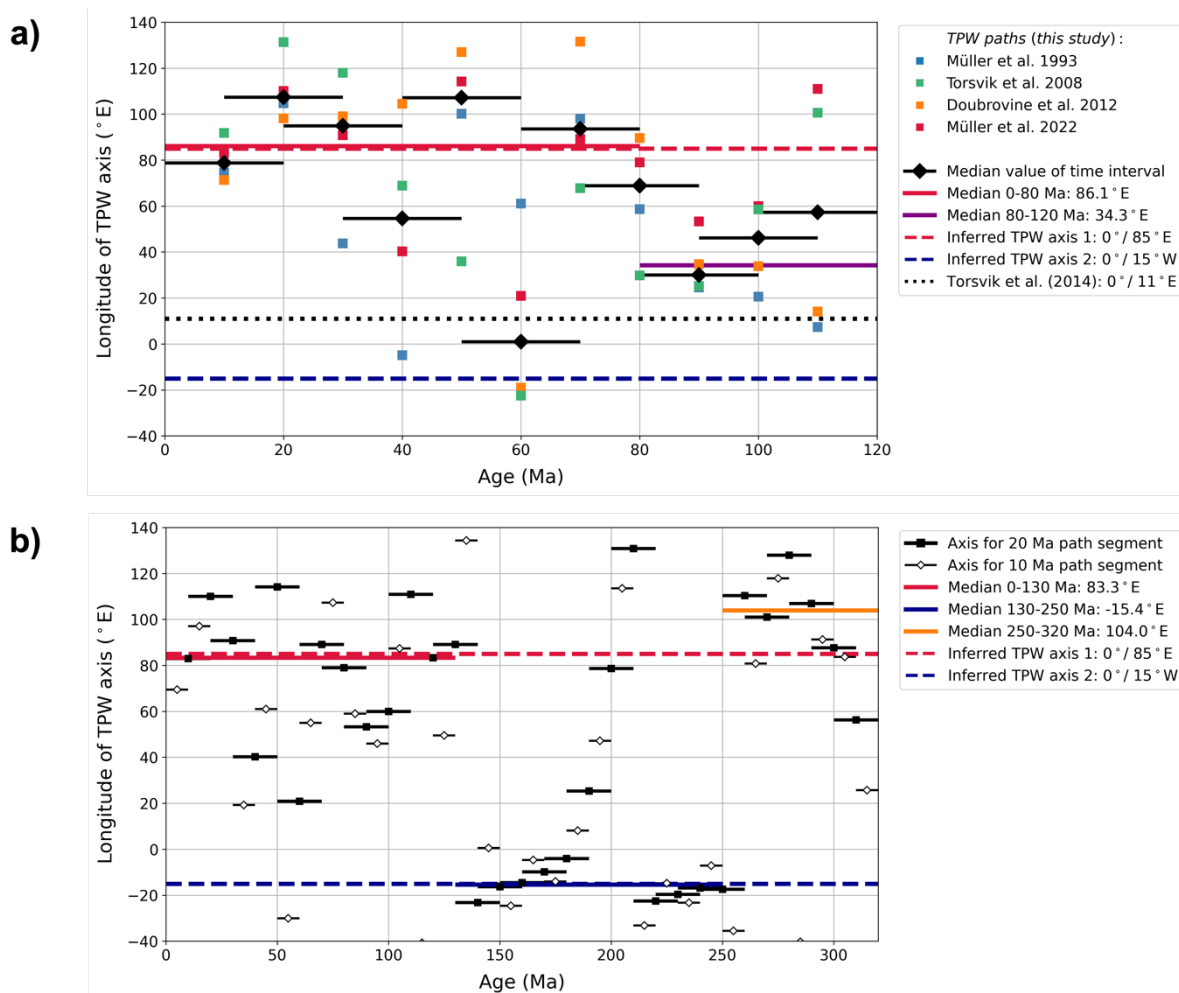
306 **4.1 True polar wander since 320 Ma**

307 We have quantified the motion of the time-averaged paleomagnetic pole relative to the mantle using
308 the global APWP of Vaes et al. (2023) and four different mantle reference frames. If these motions
309 correspond to the movement of the Earth's spin axis relative to the mantle, they quantify the
310 magnitude, rate, and direction of TPW. The similarities between the first-order geometry of the four
311 TPWPs for the last 120 Ma indicates that the observed trends in polar motion are reproducible, even
312 though these paths were constructed using mantle reference frames based on different datasets, plate
313 circuits and approaches. Our results clearly show that TPW since 120 Ma is non-negligible: each TPWP
314 yields an angular deviation of the spin axis relative to the mantle of $>5^\circ$ for both the early Cenozoic
315 (50-60 Ma) and Early Cretaceous. This would argue for a rejection of the null hypothesis that no
316 significant TPW occurred since the Late Cretaceous, in contrast to the conclusions reach in a recent
317 paper by Cottrell et al. (2023), as well as to previous TPW estimates of Torsvik et al. (2014) (Fig. 4b).
318 If the TPW rotations computed here are artifacts, this would imply a large and systematic error in
319 either the global APWP or mantle reference frames. Given the well-constrained and small uncertainty
320 of the global APWP of Vaes et al. (2023), this would suggest that there are large inadequacies in all
321 mantle reference frames used here, for instance due to a large drift of all the hotspots or large,
322 systematic errors in the relative plate motion circuit, which we consider unlikely.

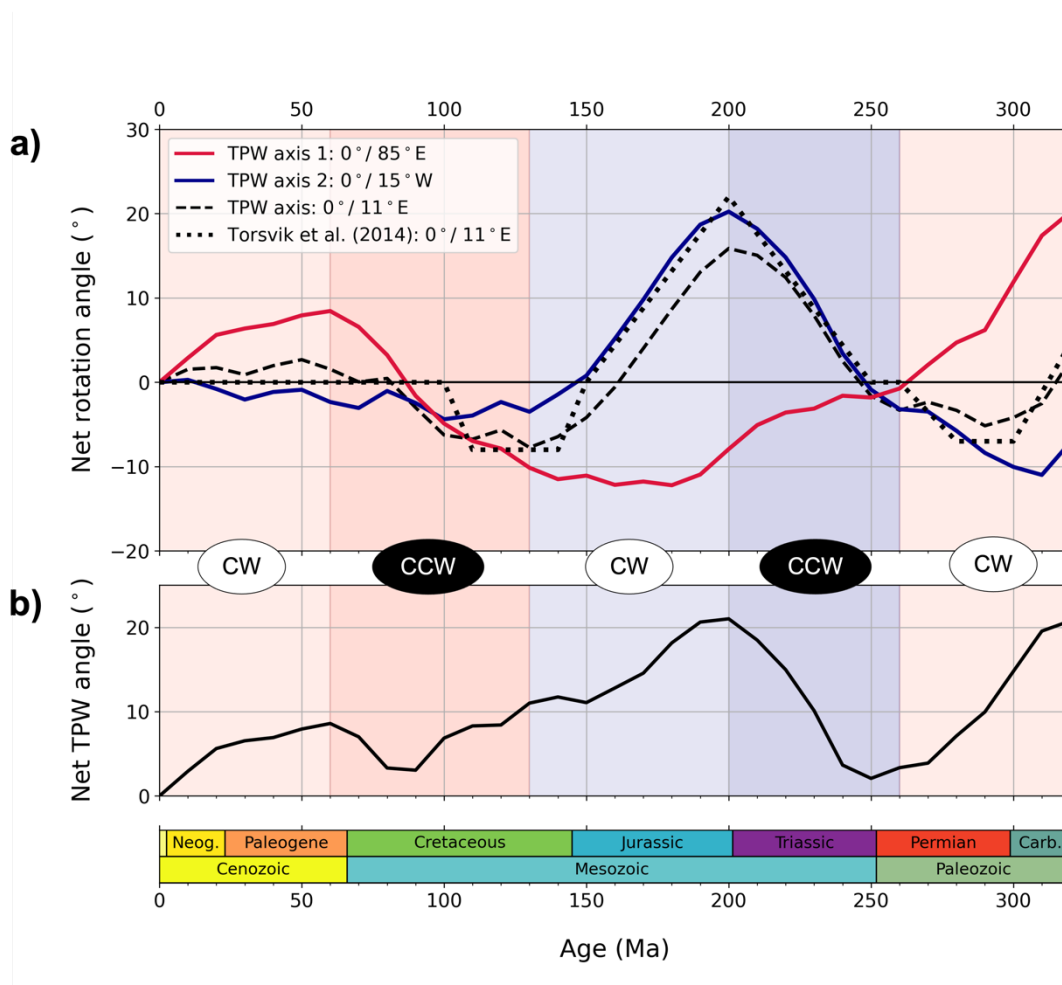
323 The four TPWPs of the last 120 Ma all indicate a back-and-forth motion of the mantle relative
324 to the spin axis during the last 80 Ma (Fig. 2a-d). This oscillatory motion was previously computed by
325 Doubrovine et al. (2012) in a comparison of their moving hotspot frame and the global APWP of
326 Torsvik et al. (2012). Intriguingly, the direction of TPW for the last 80 Ma is nearly orthogonal to the
327 great circle about an equatorial axis at 11°E (Fig. 6), which is the axis of TPW rotation that would be
328 expected if the Earth's moment of inertia is mainly controlled by the basal mantle structures referred
329 to as large low shear-wave velocity provinces (LLSVPs; Steinberger & Torsvik, 2008; Torsvik et al.,
330 2012, 2014) and that is close to the present-day TPW axis at $\sim 10^\circ\text{E}$ (e.g., Pavoni, 2008). The small
331 component of TPW about this axis for the last 80 Ma is consistent with the findings of Torsvik et al.
332 (2014), who modelled no significant TPW rotations around an equatorial axis located at $0^\circ/11^\circ\text{E}$ for
333 the last 100 Ma (Fig. 7a). Instead, our TPWP for the last 320 Ma shows a $\sim 9^\circ$ oscillatory TPW rotation
334 about an axis located at $\sim 85^\circ\text{E}$ (Figs. 6, 7a).

335 However, the estimated TPW axis between 80 and 120 Ma is closer to the $0^\circ/11^\circ\text{E}$ axis, with
336 an estimated longitude of the rotation axis based on all four TPWPs of $\sim 34^\circ$ (Fig. 6a). The TPW axis
337 determined from the three hotspot-based mantle frames is particularly in agreement with this TPW
338 axis, which is also observed from the (sub-)parallel trajectories of the TPWPs to the great-circle about
339 that axis (Fig. 2a-c). The TPWP based on the fixed hotspot frame of Müller et al. (1993) shows the
340 largest rotation of $\sim 15^\circ$ about this axis, between 80 and 120 Ma, although we note that the fixed
341 hotspot model prior to 80 Ma is considered much less reliable (e.g., Torsvik et al., 2008). The

342 previously identified phase of relatively fast TPW ($\sim 0.8^\circ/\text{Ma}$) at 110-100 Ma (Steinberger & Torsvik,
 343 2008; Torsvik et al., 2012, 2014) is, however, absent in our TPWPs (Fig. 2e). Vaes et al. (2023) showed
 344 that a spike in APW between 110 and 100 Ma in the global APWP of Torsvik et al. (2012) was likely
 345 the result of temporal bias, and we therefore interpret this inferred 110-100 Ma TPW event as a result
 346 of this artifact in the underlying APWP.
 347



348 **Fig. 6.** Estimated position of the equatorial axis of TPW. **a)** Longitude of the TPW axis computed for
 349 20 Ma segments (e.g., 0-20 Ma, 10-30 Ma) of each TPW path shown in Figs. 2a-d. The median value
 350 for each time interval is depicted with the thick black lines and diamonds. The median longitude for
 351 the 0-80 Ma and 80-120 Ma time intervals are plotted as red and purple horizontal lines. Inferred main
 352 TPW axes are shown as dashed lines. The dotted black line is the preferred axis of TPW from Torsvik
 353 et al. (2014). **b)** Longitude of the TPW axis determined for both 10 and 20 Ma segments of the TPW
 354 path for the last 320 Ma, shown in Fig. 4a. Median longitude values are shown for the 0-130, 130-250
 355 and 250-320 Ma intervals.
 356



357
 358 **Fig. 7.** Magnitude of TPW since 320 Ma. **a)** Net rotation angle around three different equatorial TPW
 359 axes. The angles are computed from the TPW path for the last 320 Ma (Fig. 4a) as the total rotation
 360 around each axis. Positive values indicate a net clockwise (CW) rotation since that time. Five major,
 361 long-term TPW rotations are identified for the last 320 Ma. Clockwise/counterclockwise (CCW)
 362 rotations around the inferred TPW axis 1 (0°/85°E) or TPW axis 2 (0°/15°W) are shown highlight by
 363 light/dark red or blue shading, respectively. The dotted black line shows the estimated net TPW
 364 rotations around the preferred TPW axis of 0°/11°E from Torsvik et al. (2014). **b)** Net TPW angle since
 365 320 Ma, computed as the difference between the pole position (that is, the spin axis) relative to the
 366 mantle (that is, the geographic pole in Fig. 4a).

367
 368 The TPWP computed for the last 320 Ma shows that TPW predominantly occurred around two
 369 equatorial rotation axes that are approximately orthogonal: one axis at ~85°E and a second axis
 370 located at ~15°W (Fig. 6). Remarkably, the timing and magnitude of true polar wander along the first
 371 axis are very similar to the TPW rotations determined by Torsvik et al. (2012, 2014) based on
 372 paleomagnetic data alone (Fig. 7), which built upon earlier work by Steinberger & Torsvik (2008). Our
 373 new TPWP shows a motion of the spin axis of ~24° away from the geographic pole between 260 and
 374 200 Ma, and back parallel to the same great circle and with similar magnitude between 200 and 130

375 Ma (Fig. 7). The inferred rotation axes at a longitude of 15°W is very close to the estimated axes by
376 Steinberger & Torsvik (2008), Torsvik et al. (2012) and Mitchell et al. (2012). These motions would
377 correspond to a coherent counterclockwise rotation of the solid Earth relative to the spin axis between
378 260 and 200 Ma, followed by a clockwise rotation between 200 and 130 Ma, in agreement with
379 previous findings of e.g., Torsvik et al. (2014). Our results confirm previous inferences by Torsvik et
380 al. (2012, 2014) that cumulative TPW for the last 250 Ma is close to zero (Fig. 7b). Finally, we observe
381 a TPW rotation of $\sim 20^\circ$ between 320 and 260 Ma, yielding an angular deviation of the spin axis relative
382 to the mantle of $\sim 20^\circ$ for the Late Carboniferous (~ 320 -310 Ma). This northward motion of Pangea
383 towards the equator has previously been interpreted as the result of TPW (e.g., Le Pichon et al., 2021).
384 However, in the approach of Torsvik et al. (2012, 2014), Africa is assumed to have remained
385 longitudinally more or less stable and the axis of TPW is fixed at $0^\circ/11^\circ\text{E}$, i.e., within Africa. With those
386 underlying assumptions, those studies cannot determine paleolatitudinal motion of Africa (and
387 Pangea) as TPW. The very low absolute plate motion of Africa (and thus Pangea) in the mantle
388 reference frame of Müller et al. (2022) (Fig. 3b), which mostly results from minimizing continent
389 motions relative to the mantle, suggests that most of Pangea's paleolatitudinal motion between 320
390 and 260 Ma is a result of TPW, which has some important implications for the structure of the deep
391 mantle that will be discussed in section 4.3.

392

393 **4.2 True polar wander: not so fast?**

394 Phases of rapid TPW are frequently proposed based on rapid shifts in paleomagnetic pole positions.
395 The existence of episodic, and possibly oscillatory, phases of rapid TPW are actively investigated by
396 the paleomagnetic community. They are particularly interesting because it may significantly impact
397 regional climate, paleoenvironment, sea level and life (e.g., Raub et al., 2007; Muttoni et al., 2013; Jing
398 et al., 2022; Wang & Mitchell, 2023; Muttoni et al., 2024). Whether such fast polar shifts truly represent
399 rapid TPW is not always straightforwardly determined, and it may often be difficult to distinguish
400 signal from noise (e.g., Evans, 2003; Kulakov et al., 2021; Cottrell et al., 2023; Domeier et al., 2023).
401 Importantly, the many inherent uncertainties in paleomagnetic data may result in a significant
402 deviation of individual paleomagnetic pole positions from the estimated time-averaged pole given by
403 an APWP, as reflected in the dispersion of poles obtained from similar-aged rocks (Rowley, 2019; Vaes
404 et al., 2022). TPW shifts derived from the data of a single tectonic plate and/or from a small number
405 of paleomagnetic poles, each based on different numbers of paleomagnetic samples/sites and thus
406 averaging the magnetic field to different extents (Vaes et al., 2022), may be prone to unrecognized
407 biases and any conclusions drawn from such analyses should be approached with caution.

408 For the last 120 Ma, all our TPWPs show a peak in TPW rate during the Late Cretaceous (~ 80 -
409 90 Ma), with a rate of 0.5 - $0.6^\circ/\text{Ma}$ (Fig. 2e). This peak coincides with a phase of fast TPW around 84
410 Ma that was already proposed decades ago (e.g., Gordon, 1983; Sager & Koppers, 2000), although
411 these results are not without controversy (e.g., Cottrell & Tarduno, 2000). A recent study by Mitchell
412 et al. (2021) argued for a phase of rapid, oscillatory TPW ($\sim 3^\circ/\text{Ma}$) between ~ 86 and 78 Ma, based on

413 high-resolution paleomagnetic records from two partly overlapping stratigraphic sections in northern
414 Italy. Their TPW rates are much higher than obtained in this study (Fig. 4b, 5b). However, Cottrell et
415 al. (2023) recently showed argued these records contain a secondary overprint overlooked by
416 Mitchell et al. (2021) and interpreted that the section was likely affected by local block rotations,
417 causing a bias in the paleomagnetic directions and casting doubt on this interpreted fast TPW event.

418 The most notable potential episode of rapid TPW is the Jurassic ‘monster’ polar shift: a $\sim 30\text{-}40^\circ$
419 shift in pole position in the APWP of North America between ~ 160 and 145 Ma (Kent et al., 2015).
420 High-quality paleomagnetic data from Adria, under the assumption that Adria was rigidly attached to
421 Africa since the opening of the Ionian Sea between 170 and 154 Ma (Channell et al., 2022), confirm a
422 $\sim 30^\circ$ shift in pole position in North American coordinates (Kent & Muttoni, 2019; Muttoni et al., 2024).
423 However, the reliability of key paleomagnetic poles from North American kimberlites as well as the
424 assumption that Adria was rigidly attached to northern Africa have been challenged (e.g., van
425 Hinsbergen et al., 2020; Kulakov et al., 2021; Mirzaei et al., 2021). Since TPW affects all tectonic plates
426 and continents simultaneously, the existence of a rapid TPW phase may be tested at different (paleo-
427)locations. Intriguingly, different paleomagnetic datasets from a range of tectonic plates provide both
428 evidence in support of fast polar motion during the Late Jurassic, such as from North China (Yi et al.,
429 2019), the Lhasa terrane (Ma et al., 2022) and the Pacific plate (Fu & Kent, 2018), or against it, such
430 as from North China (Gao et al., 2021), Greenland (Kulakov et al., 2021) and South America (Ruiz
431 González et al., 2022).

432 Our results, based on a global APWP with high spatiotemporal data coverage and with
433 propagated age uncertainty and spatial uncertainty in the underlying paleomagnetic data, do not
434 provide any evidence for rapid ($>1.0^\circ/\text{Ma}$) TPW during the last 320 Ma (Figs. 4b, 5c). We acknowledge
435 that the absence of relatively fast TPW may, in theory, be a consequence of using a 20 Ma time window
436 for the global APWP that underlies the TPWPs presented here. This may smoothen or obscure
437 potential short-term (<10 Ma) and/or small-amplitude phases of polar wander (e.g., Muttoni et al.,
438 2005, 2024; Mitchell et al., 2021). It is interesting to note, however, that the highest TPW rates are
439 observed during the middle of a long, large-amplitude TPW rotation (Fig. 4b). This is consistent with
440 theoretical inferences that the fastest TPW is expected to occur during longer term episodes of TPW
441 (Goldreich & Toomre, 1969; Tsai & Stevenson, 2007; Cottrell et al., 2023). We indeed observe that
442 TPW rate accelerates until a peak velocity is reached before decelerating again, such that the fastest
443 TPW rate during each long-term TPW rotation (see Fig. 7) is greater than the average TPW rate for
444 that rotation (Fig. 4b). Then again, even when computing a TPWP at a 5 Ma resolution and with a 10
445 Ma time window, we do not find clear evidence for TPW occurring at velocities beyond $1^\circ/\text{Ma}$. The
446 peaks in TPW rate of more than $1.0^\circ/\text{Ma}$ observed for the 5-Ma-resolution TPWP (Fig. 5c) are not
447 statistically significant and do not follow the expected velocity pattern clearly observed for the 10-
448 Ma-resolution TPWP, and we therefore conservatively interpret these as noise rather than a true
449 ‘signal’.

450 To establish whether short (<5 Ma) phases of fast TPW have occurred since the Late Paleozoic
451 requires an increase in the resolution of the APWPs used to quantify TPW, as well as the quantification
452 of the uncertainty in the mantle reference frame. Before these become available, such rapid changes
453 in pole position may instead be identified by collecting well-dated, paleomagnetic datasets from
454 sedimentary sequences with a high sampling resolution, which may provide high-resolution records
455 of shifts in the paleomagnetic declination and inclination (e.g., Mitchell et al., 2021; Vaes et al., 2021).
456 However, observed shifts in the paleomagnetic direction may result from paleomagnetic and/or
457 tectonic artifacts, and should be thoroughly tested for potential biases. The collection of multiple high-
458 resolution paleomagnetic records from stratigraphic sections of overlapping age and from different
459 tectonic plates provides a way to test whether an observed rapid polar shift may indeed represent
460 TPW. In addition, higher-resolution APWPs computed from site-level paleomagnetic data using a
461 bottom-up uncertainty propagation scheme (Gallo et al., 2023) may allow the identification of fast and
462 short-lived phases of TPW.

463

464 **4.3 Linking true polar wander and mantle dynamics**

465 The rate of TPW provides first-order kinematic constraints on the rate of mantle convection,
466 particularly on the velocity at which density anomalies, such as sinking lithospheric slabs, move
467 through the Earth's mantle. Fu et al. (2022) presented a compilation of paleomagnetically estimated
468 TPW rates since the late Mesoproterozoic (~1100 Ma), proposing a direct link between the secular
469 change of the TPW rate and the thermal structure and nature of convection in the mantle. Fast TPW
470 (>1°/Ma) has often been inferred for pre-Pangean TPW, suggesting a different geodynamic regime
471 that may correlate with the supercontinent cycle (e.g., Evans, 2003; Mitchell, 2014; Fu et al., 2022).
472 Testing pre-Mesozoic TPW hypotheses is not straightforward, as plate motion-induced polar wander
473 may be difficult to distinguish from TPW and thus obscure past TPW signals (Evans, 2003; Torsvik et
474 al., 2014). Moreover, rapid polar shifts of up to ~90° during the Early Cambrian and Ediacaran have
475 also been attributed to TPW (e.g., Kirschvink et al., 1997; Mitchell et al., 2011; Robert et al., 2017), but
476 may alternatively be explained by unusual geomagnetic field behavior (Domeier et al., 2023; Robert
477 et al., 2023).

478 Reproducing observed TPW by numerical modeling has also proven difficult, as this requires
479 detailed knowledge on the structure of the mantle, such as the volumes and distribution of subducted
480 lithospheric slabs (see Steinberger & Torsvik, 2010). Paleomagnetism-based estimates of TPW rates
481 are frequently compared to TPW speed limits inferred from geodynamic modelling. However, these
482 predictions vary substantially. For instance, Tsai and Stevenson (2007) provide a theoretical speed
483 limit of 2.4°/Ma but find a maximum TPW shift of 8° for a period of 10 Ma (corresponding to 0.8°/Ma).
484 On the other hand, Greff-Lefftz and Besse (2014) argue that TPW may occur at rates of up to 10°/Ma
485 for larger mass reorganizations. These estimates heavily rely on the choice of rheological parameters,
486 which are poorly constrained, particularly for deep geological time (Tsai & Stevenson, 2007;
487 Steinberger & Torsvik, 2010). Moreover, whether such geodynamical models used to determine the

488 magnitude and rate of TPW have slab sinking rates that are consistent with independent kinematic
489 constraints on the slab sinking velocity versus depth, such as those obtained from seismic
490 tomographic images of subducted slabs (e.g., van der Meer et al., 2018), it not always clear
491 (Steinberger & Torsvik, 2010; van der Wiel et al., 2024).

492 Recent modelling studies show that TPW rotations are likely stabilized by the contribution to
493 the moment of inertia by the two antipodal LLSVPs, with important contributions from subducted
494 slabs, whose relative contribution to the moment of inertia strongly change with depth (e.g.,
495 Steinberger & Torsvik, 2010; Steinberger et al., 2017). Observed TPW rotations about an axis of
496 minimum moment of inertia that is close to the combined center of mass of the LLSVPs suggests that
497 TPW may be controlled by these structures (Torsvik et al., 2012; 2014). TPW rotations along an axis
498 nearly orthogonal to this $0^\circ/11^\circ\text{E}$ axis (see Figs. 6, 7) instead indicate that the reorientation of the
499 solid Earth may (also) be controlled by other contributions to the moment of inertia tensor, e.g.,
500 resulting from large density anomalies caused by subducting slabs at relatively high latitudes $\sim 90^\circ$
501 from this alternative axis (Steinberger & Torsvik, 2010). If driven by changes in subduction
502 configuration and slab sinking, the two approximately orthogonal axes of TPW identified here (Figs.
503 6, 7) roughly coincide with low-latitude subduction in the Tethyan realm for the $\sim 0^\circ/15^\circ\text{E}$ axis,
504 whereas the $\sim 0/85^\circ\text{E}$ axis would correspond to changes in subduction flux in the Pacific realm. Our
505 calculations show that the magnitudes of TPW are roughly equal for the two, or even slightly larger
506 for the effects of Tethyan subduction, even though Tethyan subduction occurs at much lower latitudes
507 than Pacific subduction (e.g., Seton et al., 2012; Vaes et al., 2019; Boschman et al., 2021). This may
508 illustrate the stabilizing effects of LLSVPs and could allow the detailed computation of their absolute
509 density from their contribution to the moment of inertia.

510 Intriguingly, our results show a $\sim 20^\circ$ TPW rotation for the period between 320 and 260 Ma
511 around an axis orthogonal to $0^\circ/11^\circ\text{E}$ axis (Fig. 7a). This would identify the well-constrained
512 northward motion of Pangea during this time interval as largely a result of TPW (Marcano et al., 1999;
513 Le Pichon et al., 2021). This is surprising, given that the LLSVPs are thought to dominate the present-
514 day moment of inertia of the Earth (Steinberger & Torsvik, 2010) and may have remained stable and
515 antipodal throughout the entire Phanerozoic (Torsvik et al., 2014). If correct, this TPW rotation would
516 imply that the contribution of other density anomalies than the LLSVPs, likely high-latitude slabs, may
517 contribute sufficiently to the total moment of inertia to allow them to rotate $\sim 20^\circ$ relative to the spin
518 axis towards the equatorial plane. This could be explained by either a different mantle viscosity
519 and/or density structure during the (Late) Paleozoic, e.g., driven by a large volume of subducting slabs
520 in the upper mantle at high latitude, driving the supercontinent and its surrounding subduction zones
521 towards the equator. Alternatively, it may be explained by LLSVPs that were smaller, less dense, or
522 mobile prior to ~ 260 Ma. We note, however, that the estimates of pre-260 Ma TPW are strongly
523 influenced by the choices in either reference frame computation (the ‘optimized’ mantle reference
524 frame of Müller et al. (2022) that keeps Pangea nearly fixed to the ambient mantle to reduce

525 continental plate motion) or TPW computation (keeping the TPW axis fixed at $0^\circ/11^\circ\text{E}$, Torsvik et al.,
526 2014).

527 Finally, the computation of TPW requires knowledge of absolute plate motion in the
528 paleomagnetic and mantle reference frames. The former requires that the time-averaged geomagnetic
529 field aligns with the Earth's spin axis and that paleomagnetic data provide an accurate approximation
530 of the mean pole position. Recent analysis has shown that even higher-resolution and more precise
531 APWPs may be computed when uncertainty is propagated from site-level paleomagnetic data using a
532 bottom-up approach (Gallo et al., 2023). Moreover, we emphasize that to establish whether observed
533 TPW is statistically significant, and to assess the robustness of TPW rates and its implications for
534 mantle dynamics, it is key to improve the quantification and incorporation of uncertainties in mantle
535 reference frames. Defining a robust mantle reference frame with uncertainty quantification remains
536 a key challenge for solid Earth science. All our attempts to define a mantle reference frame will
537 inevitably remain approximations, since we are treating a convecting mantle as a fixed frame of
538 reference. However, in a mantle frame based on simple 'tectonic rules', TPW becomes an intrinsic
539 property of the mantle reference frame. This way, numerical models of global mantle convection
540 driven by plate tectonics in an assumed mantle reference frame may then be calibrated against TPW,
541 and iterated, along with hotspot tracks in an iterative modeling approach as in e.g., Doubrovine et al.
542 (2012). This may not only provide novel constraints on mantle dynamics research but also allow the
543 identification of the dynamic drivers of TPW. Lastly, we foresee that improved observational
544 constraints on the timing, rate, and magnitude of TPW will contribute to exploring the exciting links
545 between TPW and Earth's climate, hydrosphere, geodynamo, and biosphere in the geological past.

546

547 **5. Conclusions**

548 Here, we present new quantitative estimates of true polar wander since 320 Ma. We find that TPW
549 since 320 Ma occurred as large ($>10^\circ$) but slow rotations at rates typically below $0.5^\circ/\text{Ma}$, with a mean
550 TPW rate of $0.34^\circ \pm 0.14^\circ/\text{Ma}$ (1σ). The TPW paths computed using four different mantle reference
551 frames all show significant ($>5^\circ$) TPW since 100 Ma, in contrast to some recent studies. The TPW path
552 back to 320 Ma supports the existence of multiple large TPW oscillations of up to $\sim 20^\circ$ since the
553 Permian. We find no evidence for phases of fast ($>1^\circ/\text{Ma}$) TPW on timescales of >5 Ma, suggesting that
554 previously observed, and heavily debated, rapid TPW may be an artifact. Our results show that TPW
555 since 320 Ma predominantly occurred around two nearly orthogonal equatorial axes. We confirm a
556 previously constrained oscillatory TPW rotation of $\sim 24^\circ$ in the Triassic and Jurassic around an axis
557 that is close to the present-day center of mass of the antipodal LLSVPs in the lowermost mantle. In
558 contrast, TPW is shown to have occurred about an axis at $\sim 85^\circ\text{E}$ during the last ~ 80 Ma and between
559 260 and 320 Ma, implying that other contributions to the moment of inertia, such as those exerted by
560 subducting lithospheric slabs, controlled the nature of TPW. We tentatively explain the changes in the
561 dominant axis of TPW since 320 Ma to changes in the contribution to the moment of inertia of low-

562 latitude Tethyan subduction versus higher-latitude subduction in the Pacific realm. The >20° TPW
563 oscillation around an axis close to the center of LLSVPs may confirm the stabilizing effects of LLSVPs
564 on Earth's moment of inertia. Finally, we highlight that the coupling of kinematic constraints on TPW
565 with absolute plate motion models provides an opportunity for calibration of numerical experiments
566 of mantle dynamics.

567

568 **Acknowledgements**

569 This work was supported by the Netherlands Organization for Scientific Research (NWO Vici Grant
570 865.17.001) to DJJvH.

571

572 **Conflict of Interest**

573 The authors have no conflicts of interest to declare.

574

575 **Data Availability Statement**

576 The Jupyter Notebook used for the analyses in this study are publicly available on GitHub
577 (<https://github.com/bramvaes/TPW>) and will be archived on Zenodo upon acceptance of this
578 manuscript. We acknowledge the use of the freely available paleomagnetic software package PmagPy
579 (Tauxe et al., 2016) in the Python codes used to perform the calculations. The complete paleomagnetic
580 database that underpins the global APWP of Vaes et al. (2023) is available as Supplementary Datafile
581 to the online version of that publication, as well as on the Reference database portal on APWP-
582 online.org (Vaes et al., 2024).

583

584 **References**

585 Andrews, J. A. (1985). True polar wander: an analysis of Cenozoic and Mesozoic paleomagnetic
586 poles. *Journal of Geophysical Research: Solid Earth*, 90(B9), 7737-7750.

587 Besse, J., and Courtillot, V. (2002). Apparent and true polar wander and the geometry of the
588 geomagnetic field over the last 200 Myr. *Journal of Geophysical Research: Solid Earth*, 107(B11),
589 EPM-6.

590 Besse, J., Courtillot, V., Greff, M. (2021). Paleomagnetism, Polar Wander. In: Gupta, H.K. (eds)
591 Encyclopedia of Solid Earth Geophysics. Encyclopedia of Earth Sciences Series. Springer, Cham.

592 Biggin, A. J., Steinberger, B., Aubert, J., Suttie, N., Holme, R., Torsvik, T. H., ... & Van Hinsbergen, D. J. J.
593 (2012). Possible links between long-term geomagnetic variations and whole-mantle convection
594 processes. *Nature Geoscience*, 5(8), 526-533.

595 Boschman, L. M., Van Hinsbergen, D. J., Langereis, C. G., Flores, K. E., Kamp, P. J., Kimbrough, D. L., ... &
596 Spakman, W. (2021). Reconstructing lost plates of the Panthalassa Ocean through paleomagnetic
597 data from circum-Pacific accretionary orogens. *American Journal of Science*, 321(6), 907-954.

- 598 Channell, J. E., Muttoni, G., & Kent, D. V. (2022). Adria in Mediterranean paleogeography, the origin of
 599 the Ionian Sea, and Permo-Triassic configurations of Pangea. *Earth-Science Reviews*, 230, 104045.
- 600 Cottrell, R. D., & Tarduno, J. A. (2000). Late Cretaceous true polar wander: not so
 601 fast. *Science*, 288(5475), 2283-2283.
- 602 Cottrell, R. D., Bono, R. K., Channell, J. E., Bunge, H. P., & Tarduno, J. A. (2023). No Late Cretaceous true
 603 polar wander oscillation and implications for stability of Earth relative to the rotation axis. *Earth
 604 and Planetary Science Letters*, 620, 118338
- 605 Domeier, M., Robert, B., Meert, J. G., Kulakov, E. V., McCausland, P. J., Trindade, R. I., & Torsvik, T. H.
 606 (2023). The enduring Ediacaran paleomagnetic enigma. *Earth-Science Reviews*, 242, 104444.
- 607 Doubrovine, P. V., Steinberger, B., & Torsvik, T. H. (2012). Absolute plate motions in a reference frame
 608 defined by moving hot spots in the Pacific, Atlantic, and Indian oceans. *Journal of Geophysical
 609 Research: Solid Earth*, 117(B9).
- 610 Evans, D. A. (2003). True polar wander and supercontinents. *Tectonophysics*, 362(1-4), 303-320.
- 611 Fu, R. R., & Kent, D. V. (2018). Anomalous Late Jurassic motion of the Pacific Plate with implications
 612 for true polar wander. *Earth and Planetary Science Letters*, 490, 20-30.
- 613 Fu, H., Zhang, S., Condon, D. J., & Xian, H. (2022). Secular change of true polar wander over the past
 614 billion years. *Science Advances*, 8(41), eabo2753.
- 615 Gallo, L. C., Domeier, M., Sapienza, F., Swanson-Hysell, N. L., Vaes, B., Zhang, Y., ... & Van der Boon, A.
 616 (2023). Embracing uncertainty to resolve polar wander: A case study of Cenozoic North America.
 617 *Geophysical Research Letters*, 50(11), e2023GL103436.
- 618 Gao, Y., Zhang, S., Zhao, H., Ren, Q., Yang, T., Wu, H., & Li, H. (2021). North China block underwent
 619 simultaneous true polar wander and tectonic convergence in late Jurassic: New paleomagnetic
 620 constraints. *Earth and Planetary Science Letters*, 567, 117012.
- 621 Gold, T. (1955). Instability of the Earth's axis of rotation. *Nature*, 175(4456), 526-529.
- 622 Goldreich, P., & Toomre, A. (1969). Some remarks on polar wandering. *Journal of Geophysical
 623 Research*, 74(10), 2555-2567.
- 624 Gordon, R. G. (1983). Late Cretaceous apparent polar wander of the Pacific plate: evidence for a rapid
 625 shift of the Pacific hotspots with respect to the spin axis. *Geophysical Research Letters*, 10(8), 709-
 626 712.
- 627 Gradstein, F. M., Ogg, J. G., Schmitz, M. D., & Ogg, G. M. (2020). *Geologic time scale 2020*: Elsevier.
- 628 Greff-Lefftz, M., & Besse, J. (2014). Sensitivity experiments on True Polar Wander. *Geochemistry,
 629 Geophysics, Geosystems*, 15(12), 4599-4616.
- 630 Jing, X., Yang, Z., Mitchell, R. N., Tong, Y., Zhu, M., & Wan, B. (2022). Ordovician–Silurian true polar
 631 wander as a mechanism for severe glaciation and mass extinction. *Nature Communications*, 13(1),
 632 7941.
- 633 Jurdy, D. M., & Van der Voo, R. (1974). A method for the separation of true polar wander and
 634 continental drift, including results for the last 55 my. *Journal of Geophysical Research*, 79(20),
 635 2945-2952.

- 636 Kent, D. V., and Irving, E. (2010). Influence of inclination error in sedimentary rocks on the Triassic
637 and Jurassic apparent pole wander path for North America and implications for Cordilleran
638 tectonics. *Journal of Geophysical Research: Solid Earth*, 115(B10).
- 639 Kent, D. V., Kjarsgaard, B. A., Gee, J. S., Muttoni, G., & Heaman, L. M. (2015). Tracking the Late Jurassic
640 apparent (or true) polar shift in U-Pb-dated kimberlites from cratonic North America (Superior
641 Province of Canada). *Geochemistry, Geophysics, Geosystems*, 16(4), 983-994.
- 642 Kirschvink, J. L., Ripperdan, R. L., & Evans, D. A. (1997). Evidence for a large-scale reorganization of
643 Early Cambrian continental masses by inertial interchange true polar wander. *Science*, 277(5325),
644 541-545.
- 645 Kulakov, E. V., Torsvik, T. H., Doubrovine, P. V., Slagstad, T., Ganerød, M., Silkoset, P., & Werner, S. C.
646 (2021). Jurassic fast polar shift rejected by a new high-quality paleomagnetic pole from southwest
647 Greenland. *Gondwana Research*.
- 648 Le Pichon, X., Jellinek, M., Lenardic, A., Şengör, A. C., & İmren, C. (2021). Pangea migration. *Tectonics*,
649 40(6), e2020TC006585.
- 650 Livermore, R. A., Vine, F. J., & Smith, A. G. (1984). Plate motions and the geomagnetic field—II. Jurassic
651 to Tertiary. *Geophysical Journal International*, 79(3), 939-961.
- 652 Ma, Y., Wang, Q., Wang, H., Wan, B., Zhang, S., Deng, C., ... & Dekkers, M. J. (2022). Jurassic
653 paleomagnetism of the Lhasa terrane—Implications for Tethys evolution and true polar wander.
654 *Journal of Geophysical Research: Solid Earth*, 127(12), e2022JB025577.
- 655 Marcano, M. C., Van der Voo, R., & Mac Niocaill, C. (1999). True polar wander during the Permo-
656 Triassic. *Journal of Geodynamics*, 28(2-3), 75-95.
- 657 Merdith, A. S., Williams, S. E., Collins, A. S., Tetley, M. G., Mulder, J. A., Blades, M. L., ... & Müller, R. D.
658 (2021). Extending full-plate tectonic models into deep time: Linking the Neoproterozoic and the
659 Phanerozoic. *Earth-Science Reviews*, 214, 103477.
- 660 Mitchell, R. N. (2014). True polar wander and supercontinent cycles: Implications for lithospheric
661 elasticity and the triaxial Earth. *American Journal of Science*, 314(5), 966-979.
- 662 Mitchell, R. N., Kilian, T. M., & Evans, D. A. (2012). Supercontinent cycles and the calculation of absolute
663 palaeolongitude in deep time. *Nature*, 482(7384), 208-211.
- 664 Mitchell, R. N., Kilian, T. M., Raub, T. D., Evans, D. A., Bleeker, W., & Maloof, A. C. (2011). Sutton hotspot:
665 Resolving Ediacaran-Cambrian Tectonics and true polar wander for Laurentia. *American Journal*
666 *of Science*, 311(8), 651-663.
- 667 Mitchell, R. N., Thissen, C. J., Evans, D. A., Slotznick, S. P., Coccioni, R., Yamazaki, T., & Kirschvink, J. L.
668 (2021). A Late Cretaceous true polar wander oscillation. *Nature Communications*, 12(1), 3629.
- 669 Morgan, W. J. (1971). Convection plumes in the lower mantle. *Nature*, 230, 42-43.
- 670 Morgan, W. J. (1981). Hotspot tracks and the opening of the Atlantic and Indian Oceans. *The Sea, vol.*
671 *7, The Oceanic Lithosphere*, 443-487.

- 672 Müller, R. D., Flament, N., Cannon, J., Tetley, M. G., Williams, S. E., Cao, X., ... & Merdith, A. (2022). A
 673 tectonic-rules-based mantle reference frame since 1 billion years ago—implications for
 674 supercontinent cycles and plate–mantle system evolution. *Solid Earth*, *13*(7), 1127-1159.
- 675 Müller, R. D., Royer, J. Y., & Lawver, L. A. (1993). Revised plate motions relative to the hotspots from
 676 combined Atlantic and Indian Ocean hotspot tracks. *Geology*, *21*(3), 275-278.
- 677 Muttoni, G., Dallanave, E., & Channell, J. E. T. (2013). The drift history of Adria and Africa from 280 Ma
 678 to Present, Jurassic true polar wander, and zonal climate control on Tethyan sedimentary facies.
 679 *Palaeogeography, Palaeoclimatology, Palaeoecology*, *386*, 415-435.
- 680 Muttoni G., Dallanave E., & Della Porta G. (2024). European Arid Anomaly explained with southward
 681 drift of Eurasia during the Late Jurassic Polar Shift. *ESS Open Archive*. DOI:
 682 10.22541/essoar.172108263.33631771/v1
- 683 Muttoni, G., Erba, E., Kent, D. V., & Bachtadse, V. (2005). Mesozoic Alpine facies deposition as a result
 684 of past latitudinal plate motion. *Nature*, *434*(7029), 59-63.
- 685 Muttoni, G., and Kent, D. V. (2019). Jurassic monster polar shift confirmed by sequential paleopoles
 686 from Adria, promontory of Africa. *Journal of Geophysical Research: Solid Earth*, *124*(4), 3288-3306.
- 687 O'Neill, C., Müller, D., & Steinberger, B. (2005). On the uncertainties in hot spot reconstructions and
 688 the significance of moving hot spot reference frames. *Geochemistry, Geophysics, Geosystems*, *6*(4).
- 689 Pavoni, N. (2008). Present true polar wander in the frame of the Geotectonic Reference System. *Swiss*
 690 *Journal of Geosciences*, *101*, 629-636.
- 691 Raub, T. D., Kirschvink, J. L., & Evans, D. A. D. (2007). True polar wander: linking deep and shallow
 692 geodynamics to hydro-and bio-spheric hypotheses. *Treatise on geophysics*, *5*, 565-589.
- 693 Robert, B., Besse, J., Blein, O., Greff-Lefftz, M., Baudin, T., Lopes, F., ... & Belbadaoui, M. (2017).
 694 Constraints on the Ediacaran inertial interchange true polar wander hypothesis: A new
 695 paleomagnetic study in Morocco (West African Craton). *Precambrian Research*, *295*, 90-116.
- 696 Robert, B., Corfu, F., Domeier, M., & Blein, O. (2023). Evidence for large disturbances of the Ediacaran
 697 geomagnetic field from West Africa. *Precambrian Research*, *394*, 107095.
- 698 Rose, I., & Buffett, B. (2017). Scaling rates of true polar wander in convecting planets and moons.
 699 *Physics of the Earth and Planetary Interiors*, *273*, 1-10.
- 700 Rowley, D. B. (2019). Comparing paleomagnetic study means with apparent wander paths: A case
 701 study and paleomagnetic test of the Greater India versus Greater Indian Basin hypotheses.
 702 *Tectonics*, *38*(2), 722-740.
- 703 Ruiz González, V., Renda, E. M., Vizán, H., Ganerød, M., Puigdomenech, C. G., & Zaffarana, C. B. (2022).
 704 Deformation along the Deseado Massif (Patagonia, Argentina) during the Jurassic Period and its
 705 relationship with the Gondwana breakup: paleomagnetic and geochronological constraints.
 706 *Tectonophysics*, *834*, 229389.
- 707 Sager, W. W., & Koppers, A. A. A. (2000). Late Cretaceous polar wander of the Pacific plate: evidence
 708 of a rapid true polar wander event. *Science*, *287*(5452), 455-459.

- 709 Seton, M., Müller, R. D., Zahirovic, S., Gaina, C., Torsvik, T., Shephard, G., ... & Chandler, M. (2012). Global
710 continental and ocean basin reconstructions since 200 Ma. *Earth-Science Reviews*, 113(3-4), 212-
711 270.
- 712 Spada, G., Ricard, Y., & Sabadini, R. (1992). Excitation of true polar wander by subduction. *Nature*, 360,
713 452-454.
- 714 Steinberger, B., & O'Connell, R. J. (1998). Advection of plumes in mantle flow: implications for hotspot
715 motion, mantle viscosity and plume distribution. *Geophysical Journal International*, 132(2), 412-
716 434.
- 717 Steinberger, B., & Torsvik, T. H. (2008). Absolute plate motions and true polar wander in the absence
718 of hotspot tracks. *Nature*, 452(7187), 620-623.
- 719 Steinberger, B., & Torsvik, T. H. (2010). Toward an explanation for the present and past locations of
720 the poles. *Geochemistry, Geophysics, Geosystems*, 11(6).
- 721 Steinberger, B., Seidel, M. L., & Torsvik, T. H. (2017). Limited true polar wander as evidence that Earth's
722 nonhydrostatic shape is persistently triaxial. *Geophysical Research Letters*, 44(2), 827-834.
- 723 Tauxe, L., Shaar, R., Jonestrask, L., Swanson-Hysell, N. L., Minnett, R., Koppers, A. A. P., ... & Fairchild, L.
724 (2016). PmagPy: Software package for paleomagnetic data analysis and a bridge to the Magnetism
725 Information Consortium (MagIC) Database. *Geochemistry, Geophysics, Geosystems*, 17(6), 2450-
726 2463.
- 727 Tetley, M. G., Williams, S. E., Gurnis, M., Flament, N., & Müller, R. D. (2019). Constraining absolute plate
728 motions since the Triassic. *Journal of Geophysical Research: Solid Earth*, 124(7), 7231-7258.
- 729 Torsvik, T. H., Müller, R. D., Van der Voo, R., Steinberger, B., & Gaina, C. (2008). Global plate motion
730 frames: toward a unified model. *Reviews of geophysics*, 46(3).
- 731 Torsvik, T. H., van der Voo, R., Doubrovine, P. V., Burke, K., Steinberger, B., Ashwal, L. D., ... & Bull, A. L.
732 (2014). Deep mantle structure as a reference frame for movements in and on the Earth.
733 *Proceedings of the National Academy of Sciences*, 111(24), 8735-8740.
- 734 Torsvik, T. H., van der Voo, R., Preeden, U., Mac Niocaill, C., Steinberger, B., Doubrovine, P. V., et al.
735 (2012). Phanerozoic polar wander, palaeogeography and dynamics. *Earth-Science Reviews*, 114(3-
736 4), 325-368.
- 737 Tsai, V. C., & Stevenson, D. J. (2007). Theoretical constraints on true polar wander. *Journal of*
738 *Geophysical Research: Solid Earth*, 112(B5).
- 739 Vaes, B., van Hinsbergen, D. J., & Boschman, L. M. (2019). Reconstruction of subduction and back-arc
740 spreading in the NW Pacific and Aleutian Basin: Clues to causes of Cretaceous and Eocene plate
741 reorganizations. *Tectonics*, 38(4), 1367-1413.
- 742 Vaes, B., Li, S., Langereis, C. G., & van Hinsbergen, D. J. (2021). Reliability of palaeomagnetic poles from
743 sedimentary rocks. *Geophysical Journal International*, 225(2), 1281-1303.
- 744 Vaes, B., Gallo, L. C., & van Hinsbergen, D. J. (2022). On pole position: causes of dispersion of the
745 paleomagnetic poles behind apparent polar wander paths. *Journal of Geophysical Research: Solid*
746 *Earth*, 127(4), e2022JB023953.

- 747 Vaes, B., van Hinsbergen, D. J., van de Lagemaat, S. H., van der Wiel, E., Lom, N., Advokaat, E. L., ... &
748 Langereis, C. G. (2023). A global apparent polar wander path for the last 320 Ma calculated from
749 site-level paleomagnetic data. *Earth-Science Reviews*, 104547.
- 750 Vaes, B., van Hinsbergen, D., & Paridaens, J. (2024). APWP-online.org: a global reference database and
751 open-source tools for calculating apparent polar wander paths and relative paleomagnetic
752 displacements. *tektonika*, 2(1), 174–189.
- 753 Van der Meer, D. G., van Hinsbergen, D. J., & Spakman, W. (2018). Atlas of the underworld: Slab
754 remnants in the mantle, their sinking history, and a new outlook on lower mantle
755 viscosity. *Tectonophysics*, 723, 309-448.
- 756 Van der Wiel, E., van Hinsbergen, D. J., Thieulot, C., & Spakman, W. (2024). Linking rates of slab sinking
757 to long-term lower mantle flow and mixing. *Earth and Planetary Science Letters*, 625, 118471.
- 758 Van Hinsbergen, D. J., Torsvik, T. H., Schmid, S. M., Mañenco, L. C., Maffione, M., Vissers, R. L., ... &
759 Spakman, W. (2020). Orogenic architecture of the Mediterranean region and kinematic
760 reconstruction of its tectonic evolution since the Triassic. *Gondwana Research*, 81, 79-229.
- 761 Wang, C., & Mitchell, R. N. (2023). True polar wander in the Earth system. *Science China Earth Sciences*,
762 66(6), 1165-1184.
- 763 Wilson, J. T. (1963). A possible origin of the Hawaiian Islands. *Canadian Journal of Physics*, 41(6), 863-
764 870.
- 765 Yi, Z., Liu, Y., & Meert, J. G. (2019). A true polar wander trigger for the Great Jurassic East Asian
766 Aridification. *Geology*, 47(12), 1112-1116.

Slow true polar wander around varying equatorial axes since 320 Ma

B. Vaes^{1,2} and D.J.J. van Hinsbergen¹*

¹Department of Earth Sciences, Utrecht University, Utrecht, The Netherlands

²Department of Earth and Environmental Sciences, University of Milano-Bicocca, Milan, Italy

**Corresponding author: Bram Vaes (bram.vaes@unimib.it)*

Contents of this file

Figures S1 and S2

Tables S1 to S5

Introduction

The supplementary material provided in this file consists of two additional figures and five additional tables. Figure S1 shows the construction of the global APWP of Vaes et al. (2023) interpolated to exact 10 Ma and 5 Ma steps. Figure S2 shows the apparent polar rate of these interpolated APWPs and how to compare to the rates of the published global APWP of Vaes et al. (2023). Table S1 provides the Euler rotation parameters for the four mantle reference frames. The interpolated global APWP for the last 320 Ma is tabulated in South African coordinates in Table S2. Table S3 lists the polar wander paths constructed from each of the four mantle reference frames, which are shown in Figure 1. Table S4 provides the true polar wander paths computed at a 10-Ma-resolution that are plotted in Figure 2. Finally, Table S5 gives lists the interpolated global APWP and true polar wander path computed at a 5-Ma-resolution.

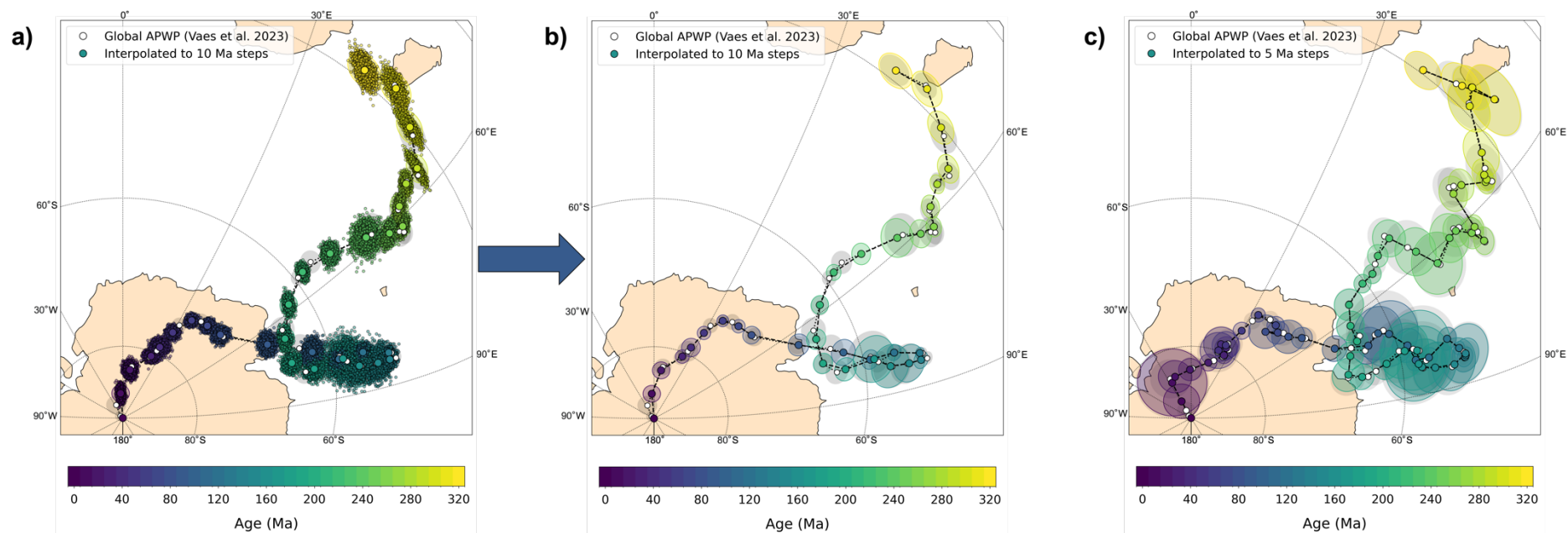


Figure S1. a) Orthographic plot showing the interpolated reference poles obtained by 1000 iterations. For each iteration, interpolated reference poles are determined at exact 10 Ma steps by interpolation along the great circle between successive reference poles. The initially computed reference poles have an ‘effective’ age computed by taking the mean age of the re-sampled virtual geomagnetic poles (VGPs) that fall within the 20 Ma window around the interpolation age. This ‘effective’ age therefore differs from the center age of the time window. See Vaes et al. (2023) for more details. **b)** The global APWP of Vaes et al. (2023) in South African coordinates (in white) compared to the interpolated path at 10 Ma steps used in this study. **c)** Same as b) but using a 5 Ma temporal resolution and a 10 Ma time window.

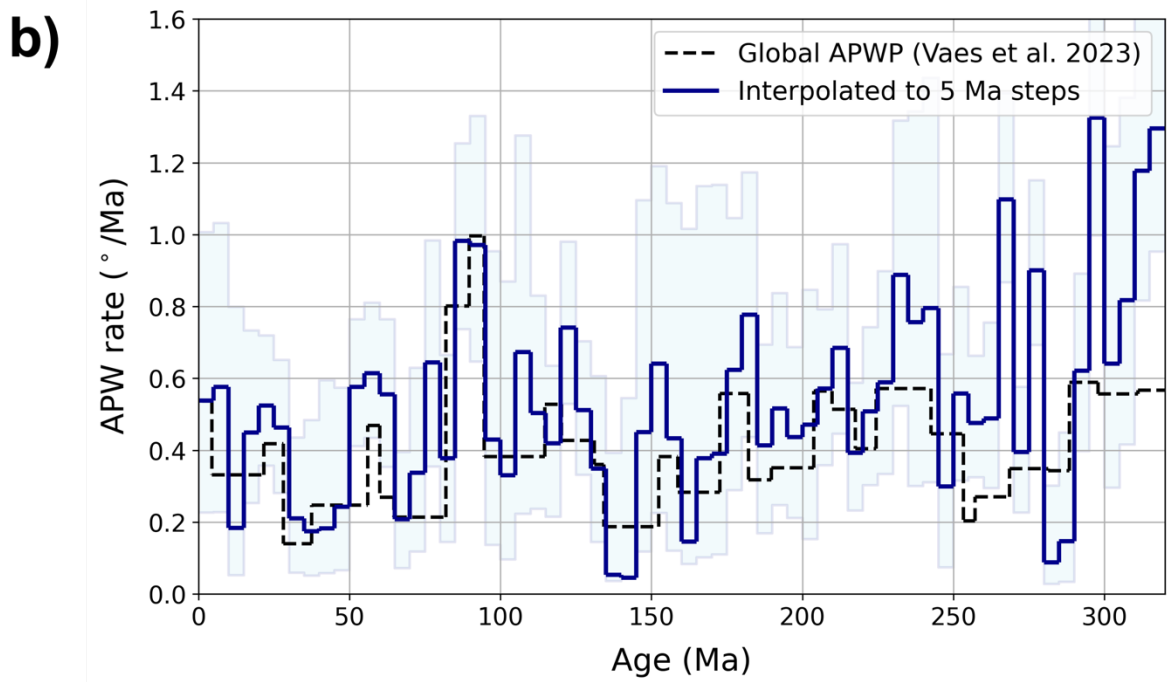
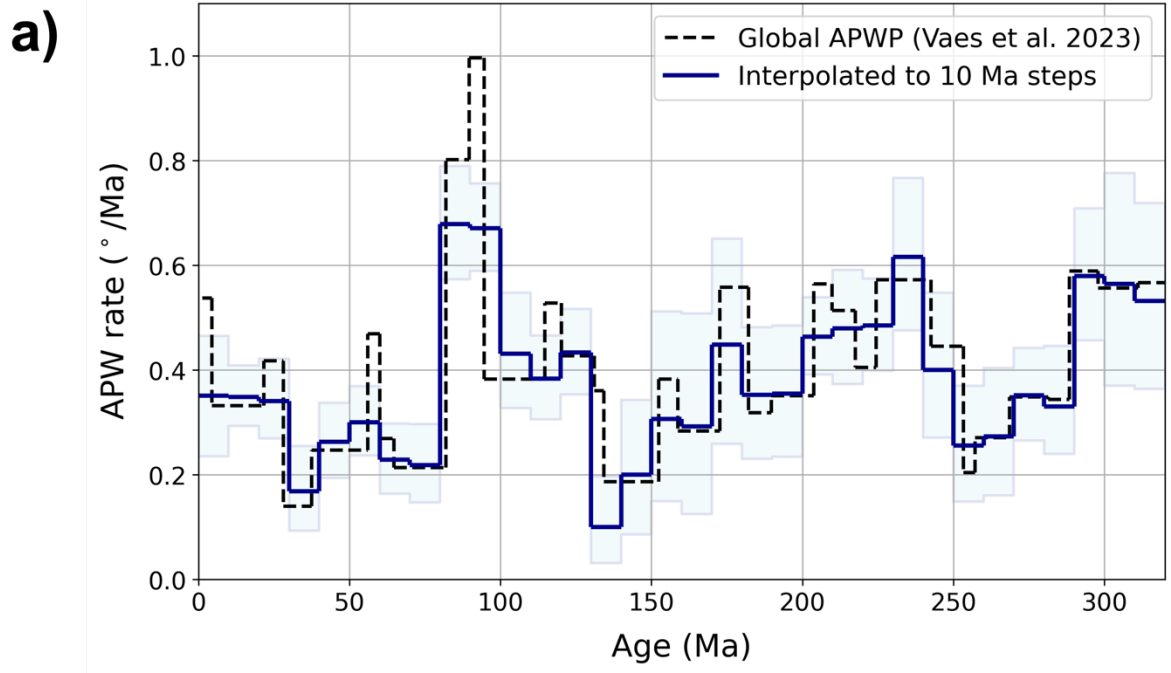


Figure S2. a) APW rates derived from the interpolated global APWP (in South African coordinates) per 10 Ma age interval (blue line). The light blue band represents the 95% confidence regions. The original APW rates obtained by Vaes et al. (2023) – corrected for the effective age – are shown by the dashed black line. **b)** Same as a) but for the 5-Ma-resolution APWP.

Müller et al. (1993)			
Age*	Lat	Lon	Angle
0	0	0	0
10.9	59.3	-31.6	-1.89
20.1	50.9	-44.5	-4.36
33.1	40.3	-43.0	-7.91
40.1	37.7	-41.2	-9.65
47.9	32.8	-40.8	-12.09
55.9	30.1	-41.7	-13.89
67.7	26.4	-40.9	-16.23
73.0	22.3	-39.6	-17.80
79.1	18.0	-38.9	-19.98
83.5	19.0	-40.9	-21.53
89.9	19.4	-41.9	-23.31
100.5	18.9	-39.5	-25.35
111.1	17.7	-39.5	-26.71
120.4	18.7	-39.7	-27.37
130.7	16.7	-37.5	-28.52

Torsvik et al. (2008)			
Age	Lat	Lon	Angle
0	0	0	0
5	30.3	326.0	-1.0
10	46.2	272.1	-1.9
15	45.8	276.8	-3.0
20	45.2	281.5	-4.0
25	44.4	286.0	-5.1
30	43.5	290.3	-6.1
35	44.3	297.9	-7.1
40	44.6	305.7	-8.1
45	40.8	303.3	-9.2
50	37.0	301.1	-10.3
55	30.6	310.1	-11.4
60	23.7	317.9	-12.5
65	22.2	319.4	-13.2
70	20.7	320.9	-13.8
75	19.2	322.4	-14.4
80	17.7	323.9	-15.0
85	16.2	325.3	-15.6
90	14.6	326.7	-16.2
95	14.5	328.6	-18.2
100	14.4	330.4	-20.1
105	15.1	331.1	-22.5
110	15.7	331.7	-24.9
115	16.4	332.4	-27.3
120	17.0	333.0	-29.7
125	17.5	333.5	-32.1
130	18.0	334.0	-34.6

Dubrovine et al. (2012)			
Age	Lat	Lon	Angle
0	0	0	0
10	-36.66	146.72	1.61
20	-35.58	156.74	3.52
30	-36.19	153.99	5.85
40	-37.63	147.30	9.09
50	-42.80	147.61	9.83
60	-56.84	149.31	11.47
70	-51.40	149.04	15.75
80	-30.59	156.20	19.06
90	-22.76	156.10	21.48
100	-16.58	156.03	24.22
110	-17.11	155.90	26.11
120	-17.57	155.79	28.01

Müller et al. (2022)			
Age	Lat	Lon	Angle
0	0	0	0
5	90.00	0.00	0.00
10	69.69	-51.67	-1.31
15	68.18	-50.15	-2.54
20	68.94	-48.57	-3.65
25	69.64	-45.38	-4.74
30	63.92	-42.45	-5.97
35	59.78	-40.73	-6.97
40	55.01	-37.80	-7.89
45	51.56	-34.44	-9.04
50	49.64	-33.01	-10.25
55	48.67	-33.70	-11.78
60	48.17	-35.10	-12.94
65	46.56	-36.43	-13.41
70	44.77	-37.64	-13.72
75	42.55	-37.84	-14.67
80	40.07	-37.18	-16.47
85	37.78	-38.14	-18.70
90	35.16	-39.60	-21.37
95	32.25	-39.04	-24.34
100	29.83	-38.33	-26.80
105	28.90	-37.59	-29.11
110	27.33	-35.89	-31.12
115	25.86	-34.34	-33.12
120	24.25	-33.33	-35.60
125	22.21	-32.16	-38.07
130	20.85	-32.21	-39.55
135	19.28	-32.26	-41.09
140	18.35	-32.19	-42.55
145	18.64	-31.31	-43.27
150	19.46	-30.87	-43.75
155	20.55	-30.68	-43.91
160	20.05	-30.90	-44.28
165	19.22	-30.60	-44.91
170	18.50	-30.13	-45.90
175	17.65	-29.93	-46.46
180	17.43	-29.19	-46.46
185	17.09	-28.35	-46.36

190	17.04	-28.07	-46.51
195	17.02	-27.49	-46.73
200	16.67	-27.55	-47.06
205	16.33	-27.63	-47.41
210	16.00	-29.05	-47.17
215	15.65	-30.57	-46.96
220	15.24	-32.45	-47.05
225	14.77	-34.41	-47.23
230	14.47	-35.53	-47.35
235	14.13	-36.74	-47.51
240	13.15	-36.69	-47.22
245	12.06	-36.66	-46.90
250	11.00	-36.57	-46.68
255	9.86	-36.47	-46.42
260	10.33	-36.43	-46.53
265	10.83	-36.33	-46.61
270	10.83	-36.31	-46.58
275	10.83	-36.28	-46.51
280	10.65	-36.32	-46.49
285	10.32	-36.43	-46.51
290	9.83	-36.33	-46.63
295	9.29	-36.23	-46.79
300	9.08	-36.24	-46.68
305	8.82	-36.25	-46.57
310	8.59	-36.26	-46.50
315	8.30	-36.33	-46.40
320	8.00	-36.39	-46.42

Table S1. Euler rotation parameters of the mantle reference frames used in this study, representing the total reconstruction poles of South Africa relative to the ambient mantle. Ages in million years ago (Ma). Lat/lon = latitude/longitude (in degrees). Angle in degrees; a positive angle indicates a counterclockwise rotation. * The ages of the Indo-Atlantic fixed hotspot frame of Müller et al. (1993) were updated by Torsvik et al. (2008).

Age	P ₉₅	Longitude	Latitude	APW rate	APW rate (low)	APW rate (high)
0	0.00	0.0	-90.0			
10	1.18	355.15	-86.49	0.35	0.24	0.47
20	1.17	8.04	-83.18	0.35	0.29	0.41
30	0.92	23.84	-80.58	0.34	0.27	0.42
40	1.27	26.93	-78.99	0.17	0.09	0.26
50	0.91	29.89	-76.44	0.26	0.19	0.34
60	0.80	35.08	-73.75	0.30	0.24	0.37
70	0.91	42.69	-73.05	0.23	0.16	0.30
80	1.21	50.00	-72.67	0.22	0.15	0.30
90	1.50	65.09	-68.10	0.68	0.57	0.79
100	1.79	74.39	-62.61	0.67	0.59	0.76
110	1.33	79.35	-59.04	0.43	0.33	0.55
120	1.11	79.97	-55.22	0.38	0.31	0.47
130	0.77	82.41	-51.14	0.43	0.35	0.52
140	1.21	84.01	-51.09	0.10	0.03	0.20
150	2.61	83.81	-53.08	0.20	0.09	0.34
160	3.00	82.93	-56.11	0.31	0.15	0.51
170	3.23	79.62	-58.42	0.29	0.12	0.51
180	1.62	79.54	-62.91	0.45	0.26	0.65
190	1.40	75.06	-65.85	0.35	0.23	0.48
200	1.40	66.45	-65.56	0.36	0.23	0.49
210	1.27	57.95	-62.76	0.46	0.39	0.54
220	1.08	53.54	-58.48	0.48	0.37	0.59
230	1.45	54.97	-53.70	0.48	0.40	0.58
240	2.63	57.95	-47.83	0.62	0.48	0.77
250	1.90	60.64	-44.30	0.40	0.27	0.55
260	1.38	61.41	-41.80	0.26	0.15	0.37
270	1.58	58.24	-40.47	0.27	0.16	0.40
280	1.29	56.36	-37.27	0.35	0.26	0.44
290	1.99	56.13	-33.97	0.33	0.24	0.45
300	2.38	50.95	-30.18	0.58	0.46	0.71
310	2.67	45.75	-26.88	0.56	0.37	0.78
320	2.71	39.94	-28.21	0.53	0.36	0.72

Table S2. Interpolated global APWP for the last 320 Ma in South African coordinates, calculated using a 20 Ma window. The P₉₅ represents the 95% confidence region of the reference pole (in degrees). APW rates (with their 95% confidence limits) are given in degrees/Ma. Note that the APW rate provided for e.g., 30 Ma is the rate determined for the interval between 30 and 20 Ma.

Age	M93		T08		D12		M22	
	Plon	Plat	Plon	Plat	Plon	Plat	Plon	Plat
0	0	-90	0	-90	0	-90	0	-90
10	59.15	-89.11	2.79	-88.68	57.20	-88.71	41.04	-89.05
20	47.23	-87.27	12.92	-87.18	67.76	-87.14	46.84	-88.35
30	49.17	-84.75	22.40	-85.58	65.72	-85.28	52.29	-86.49
40	51.73	-82.39	38.55	-84.23	60.08	-82.80	59.10	-84.38
50	52.27	-79.36	34.20	-81.78	60.95	-82.79	60.72	-82.23
60	52.15	-77.12	50.42	-78.56	64.12	-83.73	58.45	-80.79
70	53.23	-74.64	53.35	-77.09	65.21	-80.19	57.13	-79.20
80	53.87	-70.73	56.19	-75.71	71.08	-73.61	57.62	-75.25
90	52.05	-68.01	58.75	-74.33	70.30	-70.21	57.52	-69.46
100	54.55	-66.13	62.92	-70.54	69.53	-66.80	59.57	-64.58
110	54.63	-64.73	65.12	-66.04	69.80	-65.06	63.05	-60.28
120	54.76	-64.12	67.43	-61.63	70.10	-63.32	65.27	-54.85
130							64.79	-51.31
140							65.92	-49.10
150							67.37	-49.02
160							67.14	-47.71
170							67.48	-45.85
180							68.82	-45.80
190							69.72	-45.43
200							69.41	-44.61
210							66.12	-44.88
220							61.95	-44.42
230							59.39	-44.01
240							58.52	-44.19
250							57.73	-44.30
260							58.30	-44.26
270							58.33	-44.36
280							57.98	-44.28
290							57.77	-43.86
300							57.53	-44.01
310							57.22	-44.11
320							56.78	-44.01

Table S3. Polar wander paths constructed from the mantle reference frames in Table S1, plotted in Fig. 1. Plon/plat = pole longitude and latitude of the spin axis relative to a fixed South Africa plate in the absence of TPW. M93= Müller et al. (1993); T08 = Torsvik et al. (2008); D12 = Doubrovine et al. (2012); M22 = Müller et al. (2022).

Age	P ₉₅	M93		T08		D12		M22	
		Plon	Plat	Plon	Plat	Plon	Plat	Plon	Plat
0	0.00	0.0	90.0	0.0	90.0	0.0	90.0	0.0	90.0
10	1.18	159.4	86.8	169.2	87.8	152.8	86.9	159.4	87.1
20	1.17	164.6	85.0	-178.2	86.0	161.4	84.1	173.1	84.4
30	0.92	173.6	84.8	-159.1	85.0	172.5	83.3	-176.8	83.5
40	1.27	163.4	84.8	-170.9	84.5	163.4	83.7	174.5	83.1
50	0.91	156.2	84.5	-162.8	84.6	176.8	81.7	171.4	82.1
60	0.80	164.7	84.6	-179.6	84.0	-170.0	78.8	-179.3	81.4
70	0.91	159.4	86.7	-170.9	85.1	-174.6	81.3	-169.3	83.0
80	1.21	77.7	87.7	-160.4	86.5	149.8	83.8	-176.9	86.7
90	1.50	-38.7	85.1	-104.2	83.5	-161.9	87.2	-68.4	86.9
100	1.79	-56.9	80.8	-86.9	80.9	-88.9	85.3	-54.6	83.1
110	1.33	-58.4	77.1	-72.1	80.4	-77.1	82.5	-43.2	81.7
120	1.11	-67.7	74.6	-70.2	80.9	-82.2	80.5	-31.0	81.6
130	0.77							-33.3	79.0
140	1.21							-21.9	78.3
150	2.61							-11.0	78.9
160	3.00							8.5	77.2
170	3.23							26.7	75.4
180	1.62							38.7	71.8
190	1.40							49.1	69.4
200	1.40							58.8	69.0
210	1.27							64.6	71.5
220	1.08							66.4	75.0
230	1.45							62.2	79.9
240	2.63							54.2	86.3
250	1.90							-39.8	87.9
260	1.38							-87.2	86.6
270	1.58							-131.9	86.1
280	1.29							-141.3	82.9
290	1.99							-138.1	80.0
300	2.38							-152.9	75.2
310	2.67							-161.9	70.4
320	2.71							-175.8	69.2

Table S4. True polar wander paths computed by placing the interpolated global APWP into the mantle reference frames in Table S1, as plotted in Fig. 2a-d and Fig. 4a. The P₉₅ represents the paleomagnetic uncertainty only and is thus a minimum confidence region. See captions of the tables above for the meaning of the abbreviations.

Age	P ₉₅	Interpolated APWP at 5 Ma steps					TPWP	
		Plon	Plat	APW rate	APW rate (low)	APW rate (high)	Plon	Plat
0	0.00	0.0	-90.0	0.54	0.23	1.01	0.0	90.0
5	2.42	331.46	-87.31	0.58	0.23	1.03	140.73	87.45
10	4.79	332.79	-84.43	0.18	0.05	0.80	140.91	84.71
15	2.26	339.52	-83.82	0.45	0.25	0.73	144.29	84.28
20	1.72	358.76	-83.21	0.52	0.36	0.72	162.21	84.18
25	1.16	16.61	-81.93	0.46	0.28	0.65	177.46	83.94
30	1.09	26.85	-80.24	0.21	0.06	0.44	-171.94	83.23
35	1.48	26.00	-79.20	0.17	0.05	0.48	-178.24	82.79
40	2.36	21.49	-79.01	0.18	0.06	0.59	166.99	82.62
45	2.24	21.40	-79.92	0.24	0.07	0.57	153.50	83.50
50	1.89	24.89	-78.89	0.58	0.41	0.76	152.94	83.40
55	1.15	29.69	-76.20	0.61	0.43	0.81	166.22	82.35
60	0.87	33.02	-73.25	0.56	0.35	0.76	178.65	80.71
65	1.14	42.55	-72.99	0.21	0.07	0.39	-164.71	82.02
70	1.50	45.63	-73.53	0.34	0.12	0.63	-164.06	83.74
75	2.19	40.71	-74.55	0.64	0.35	0.98	163.01	84.93
80	2.23	50.61	-72.90	0.38	0.14	0.67	-176.65	86.97
85	1.39	55.05	-71.58	0.98	0.74	1.25	-162.33	88.91
90	1.76	66.25	-68.48	0.97	0.65	1.33	-58.94	86.72
95	2.55	70.87	-63.99	0.43	0.14	0.95	-67.82	84.12
100	3.64	68.87	-62.05	0.33	0.10	0.87	-71.69	85.12
105	4.60	70.61	-60.62	0.67	0.22	1.28	-61.47	85.26
110	2.48	75.86	-58.55	0.50	0.24	0.83	-51.01	83.27
115	1.52	80.42	-57.80	0.42	0.21	0.63	-32.82	81.35
120	1.32	81.03	-55.74	0.74	0.53	0.98	-27.48	81.00
125	1.63	78.49	-52.35	0.51	0.33	0.70	-39.71	81.86
130	0.93	81.62	-50.69	0.35	0.14	0.61	-36.08	79.41
135	1.47	84.05	-49.89	0.05	0.04	0.39	-30.97	77.61
140	2.30	83.69	-49.75	0.05	0.04	0.55	-28.56	78.45
145	3.80	83.34	-49.75	0.45	0.12	1.10	-27.54	79.17
150	3.78	84.82	-51.80	0.64	0.23	1.19	-18.02	78.57
155	3.60	83.99	-54.97	0.43	0.12	1.09	-0.84	77.74
160	3.97	82.75	-57.02	0.15	0.08	1.02	11.96	76.74
165	5.01	81.68	-57.46	0.38	0.10	1.13	18.94	76.13
170	5.27	78.18	-57.32	0.39	0.11	1.14	26.66	76.78
175	3.84	76.94	-59.16	0.62	0.29	1.05	35.06	75.62
180	1.96	78.48	-62.19	0.78	0.44	1.17	39.22	72.70

185	1.82	79.93	-66.02	0.41	0.17	0.69	42.57	68.81
190	2.40	77.58	-67.87	0.52	0.25	0.84	47.66	67.19
195	1.98	71.38	-66.88	0.44	0.21	0.69	53.42	68.13
200	1.51	67.85	-65.23	0.47	0.15	0.85	57.19	69.36
205	2.06	62.25	-65.10	0.57	0.36	0.79	60.77	69.44
210	2.13	56.48	-63.71	0.69	0.45	0.97	65.53	70.40
215	1.20	54.33	-60.43	0.39	0.23	0.59	67.85	73.23
220	1.41	54.21	-58.47	0.51	0.30	0.74	65.20	75.17
225	1.59	51.85	-56.27	0.59	0.33	0.90	70.13	76.72
230	2.75	50.91	-53.37	0.89	0.52	1.32	74.86	79.11
235	3.50	57.46	-51.42	0.76	0.30	1.34	55.09	82.60
240	4.58	62.58	-49.51	0.80	0.31	1.44	22.06	84.01
245	3.73	60.19	-45.86	0.30	0.07	0.67	7.79	87.81
250	2.38	60.00	-44.37	0.56	0.32	0.85	-37.30	88.37
255	2.07	62.46	-42.24	0.48	0.33	0.66	-71.18	86.15
260	1.85	65.17	-40.98	0.49	0.29	0.76	-71.57	83.98
265	1.80	61.96	-41.32	1.10	0.87	1.39	-87.77	86.00
270	2.36	54.66	-41.23	0.39	0.23	0.58	-172.89	85.86
275	2.09	54.71	-39.25	0.90	0.69	1.15	-159.23	84.27
280	1.64	57.68	-35.42	0.09	0.03	0.30	-132.42	81.13
285	1.49	57.56	-34.99	0.15	0.03	0.45	-132.18	80.90
290	2.15	56.67	-34.89	0.62	0.40	0.89	-135.96	80.99
295	3.35	53.93	-32.77	1.33	1.00	1.69	-145.96	78.46
300	3.95	47.92	-28.62	0.64	0.30	1.25	-159.70	72.80
305	3.24	46.78	-25.58	0.82	0.42	1.38	-158.45	69.62
310	5.06	50.84	-23.81	1.18	0.82	1.65	-146.36	69.04
315	3.40	45.23	-26.81	1.30	0.95	1.70	-162.55	70.30
320	2.92	38.49	-29.37	0.54	0.23	1.01	179.38	69.37

Table S5. Interpolated global APWP (in South African coordinates) at a 5-Ma-resolution (shown in Fig. S1c) and true polar wander path computed at a 5-Ma-resolution that was constructed using the mantle reference frame of Müller et al. (2022). See captions of tables above for the meaning of the abbreviations.